

Hybrid Nanoadsorbents for Extraction and Separation of Rare Earth Elements in Solution

Elizabeth Polido Legaria

*Faculty of Natural Resources and Agricultural Sciences
Department of Chemistry and Biotechnology
Uppsala*

Licentiate Thesis
Swedish University of Agricultural Sciences
Uppsala 2016

Acta Universitatis Agriculturae Sueciae

Cover: Scheme for the proposed action mechanism of the prepared
nanoadsorbents. (by E. P. Legaria)

ISBN (print version) 978-91-576-9365-5
ISBN (electronic version) 978-91-576-9366-2
© 2016 Elizabeth Polido Legaria, Uppsala
Print: SLU Service/Repro, Uppsala 2016

Hybrid Nanoadsorbents for Extraction and Separation of Rare Earth Elements in Solution

Abstract

Rare Earth Elements (REE) are a group of 17 metals (those known as lanthanides plus Yttrium and Scandium), which are increasingly important for many emerging modern applications. This work is focused on the development of high performance new magnetic silica based nanoadsorbents which are surface functionalized for efficient uptake and separation of REE in solution. In the first step, three different organic reactants (organosilane derivatives) were synthesized and grafted onto the surface of custom synthesized silica (SiO₂) nanoparticles (NPs). The effective grafting was checked by ¹³C and ²⁹Si CP-MAS solid state NMR spectroscopy and FTIR spectroscopy. These hybrid nanomaterials were used as models for adsorption of REE in solution and their uptake capacity towards REE (La³⁺, Dy³⁺ and Nd³⁺) was checked via complexometric titrations with model solutions. The materials were also characterized by SEM-EDS and TEM microscopy.

In the second part of the work, one of the organic reactants previously synthesized, which displayed the best properties, was used to functionalize the surface of custom-produced core-shell magnetic silica based nanoadsorbents, consisting of a core of γ -Fe₂O₃ nanoparticles covered by a protective thin layer of SiO₂. Magnetic nanoadsorbents exhibit many attractive opportunities for industrial purposes due to their easy removal and possibility of reusing the material. These magnetic silica based nanoadsorbents were also characterized by SEM-EDS and TEM microscopy, FTIR spectroscopy and TGA analysis. The uptake efficiency was checked via complexometric titration and selectivity with binary mixtures of REE was also studied, showing a very noteworthy selectivity towards heavier REE. These results were confirmed by X-ray single crystal structure studies of the model compounds.

Lastly, a preliminary overview on the potential application of these hybrid nanoadsorbent in real industrial leachate solutions was provided. This last part of the work is still being carried out and optimized, being one of the most important and challenging future prospects for this PhD project.

Keywords: Rare Earth Elements, silica nanoparticles, hybrid nanoadsorbents, magnetite nanoparticles, selective extraction, surface functionalization, adsorption

Author's address: Elizabeth Polido Legaria, SLU, Department of Chemistry and Biotechnology, P.O. Box 7015, 750 07 Uppsala, Sweden,
E-mail: elizabeth.polido.legaria@slu.se

Dedication

A mi hermana Cristina, por tener el corazón más grande del mundo y por siempre creer en mí como nadie más.

If you ever need a helping hand, it's at the end of your arm. As you get older, remember you have another hand: The first is to help yourself; the second is to help others.

Audrey Hepburn.

Contents

List of Publications	9
Abbreviations	11
1 Introduction	13
1.1 Rare Earth Elements. Why are they so important?	14
1.2 Rare Earth Elements. Abundance and occurrence in nature	16
1.3 Magnetic Iron Oxide Nanoparticles	18
1.3.1 Iron Oxides	18
1.3.2 Magnetic behaviour of iron oxides and MNPs	18
1.3.3 MNPs as novel nanoadsorbents	19
2 Research objectives	23
3 Experimental	25
3.1 Synthesis of organic ligands (Paper I)	25
3.1.1 Synthesis of Dimethyl Iminodiacetate	26
3.1.2 Synthesis of L1	26
3.1.3 Synthesis of pyridine-2,6-dicarbonyl dichloride	27
3.1.4 Synthesis of L2	27
3.1.5 Synthesis of L3	27
3.2 Synthesis of SiO ₂ nanoparticles (SNPs)	28
3.3 Synthesis of Fe ₃ O ₄ MNPs (Paper II)	29
3.4 Synthesis of SiO ₂ coated γ -Fe ₂ O ₃ core-shell MNPs (Paper II)	29
3.5 Synthesis of organic ligand grafted SiO ₂ NPs and organic ligand grafted core-shell γ -Fe ₂ O ₃ @SiO ₂ MNPs	30
3.6 Leaching test over acidic media of γ -Fe ₂ O ₃ @SiO ₂ NPs	30
3.7 Synthesis of molecular model compounds (IDA-RE ³⁺) (Paper II)	31
3.8 REE uptake and release studies on ligand grafted SiO ₂ and γ -Fe ₂ O ₃ @SiO ₂ NPs (Paper I & II)	31
3.8.1 Static adsorption studies	31
3.8.2 Dynamic adsorption studies	32
3.8.3 Desorption studies	32
3.8.4 Complexometric titrations of RE (Dy ³⁺ , Nd ³⁺ , La ³⁺) in mother liquor over organic ligand-grafted NPs	32

3.9	Materials characterization	33
3.9.1	Solution ^1H -NMR and ^{13}C -NMR for the organic reactants (Paper I)	33
3.9.2	Solid state ^{29}Si and ^{13}C NMR for the ligand grafted SiO_2 NPs (Paper I)	33
3.9.3	Nitrogen sorption for Specific Surface Area (SSA) analysis (Paper I)	34
3.9.4	Thermal analysis (Paper I & II)	34
3.9.5	Particle size distribution and surface charge analysis (Paper I)	34
3.9.6	Photoluminescence studies of ligand grafted SiO_2 NPs bearing RE trivalent cations (Paper I)	34
3.9.7	IR spectroscopy (Paper I & II)	35
3.9.8	SEM and TEM microscopy (Paper I & II)	35
3.9.9	X-ray diffraction (Paper I & II)	36
4	Results and Discussion	37
4.1	Solution ^1H -NMR and ^{13}C -NMR for the organic ligands and the intermediates (Paper I)	37
4.2	Confirmation of ligand grafting onto the surface of the NPs	42
4.2.1	Solid state ^{29}Si and ^{13}C NMR for ligand grafted SiO_2 NPs (Paper I)	42
4.2.2	FTIR Spectroscopy (Paper I & II)	44
4.2.3	Thermo-gravimetric analysis (TGA) (Paper I & II)	47
4.3	Surface morphology and composition (SEM and TEM microscopy) (Paper I & II)	49
4.3.1	SiO_2 NPs and ligand-grafted SiO_2 NPs (Paper I)	49
4.3.2	Ligand-grafted magnetic $\gamma\text{-Fe}_2\text{O}_3@\text{SiO}_2$ MNPs (Paper II)	52
4.4	Stability of $\gamma\text{-Fe}_2\text{O}_3@\text{SiO}_2$ NPs. Leaching test (Paper II)	53
4.5	RE3+ adsorption kinetic curves	54
4.5.1	Ligand grafted SiO_2 NPs (Paper I)	54
4.5.2	Ligand grafted $\gamma\text{-Fe}_2\text{O}_3@\text{SiO}_2$ MNPs (Paper II)	55
4.6	Desorption and selectivity studies (Paper I & II)	56
4.6.1	Molecular insights into the observed selectivity (Paper II)	57
4.7	Testing on real solutions. Industrial leachate from Fen Minerals	58
5	Conclusions	61
6	Future prospects	63

References	65
Acknowledgements	73

List of Publications

This thesis is based on the work contained in the following papers, referred to by Roman numerals in the text:

- I S. D. Topel, E. P. Legaria, C. Tiseanu, J. Rocha, J-M. Nedelec, V. G. Kessler, G. A. Seisenbaeva (2014). Hybrid silica nanoparticles for sequestration and luminescence detection of trivalent rare-earth ions (Dy^{3+} and Nd^{3+}) in solution. *Journal of Nanoparticle Research* 16: 2783.
- II E. P. Legaria, S. D. Topel, V. G. Kessler, G. A. Seisenbaeva (2015). Molecular insights into the selective action of a magnetically removable complexone-grafted adsorbent. *Dalton Transactions* 44, 1273-1282.

Papers I and II are reproduced with the permission of the publishers.

Abbreviations

APTES	3-aminopropyltriethoxysilane
DCM	Dichloromethane
DIPEA	N,N-diisopropylethylamine
EDS	Energy Dispersive Spectroscopy
EDTA	Ethylenediaminetetraacetic acid
FTIR	Fourier-transform infrared
HREE	Heavy Rare Earth Elements
ICPTES	3-isocyanatopropyltriethoxysilane
IDA	Iminodiacetic acid
IDA-RE ³⁺	Iminodiacetic acid binded with Rare Earth trivalent cations
IPTES	3-iodopropyltriethoxysilane
L1	Ligand 1
L2	Ligand 2
L3	Ligand 3
LREE	Light Rare Earth Elements
MAS	Magic Angle Spinning
MNPs	Magnetic Nanoparticles
NMR	Nuclear Magnetic Resonance
RE ³⁺	Trivalent Rare Earth cations
REE	Rare Earth Elements
SEM	Scanning Electron Microscopy
SiO ₂ NPs	Silica Nanoparticles
SNPs	SiO ₂ nanoparticles
SSA	Specific Surface Area
TEA	Trimethylamine
TEM	Transmission Electron Microscopy
TEOS	Tetraethyl ortosilicate
TGA	Thermo-gravimetric analysis

1 Introduction

Rare Earth Elements (REE) have lately gained an increasing importance for current society. In June 2010, the European Commission published a list of 14 materials (metals or group of metals) that are critical for many emerging technologies. The list included Rare Earth metals group (European Commission, 2010). This group of metals might be not so widely known because they are used in small quantities, but they are indeed essential for hundreds of varied high tech applications ranging from high field strength magnets to numerous medical applications that overall, define the basis of our modern life to a greater or lesser extent, becoming thus indispensable for the development of technology. Therefore, it is not surprising that this has resulted in an increased demand for REE as raw materials and hence an increase in their ore production (mining) and research interest in the development of efficient procedures for their extraction and separation and recycling strategies.

Several methods have been developed and are currently under the attempt of being optimized, such as solvent extraction, ionic liquids, ion-exchange resins or novel adsorbent materials with high affinity towards REE. This work focuses on the last mentioned technique, having the aim of developing new hybrid nanoadsorbents highly efficient and selective for the extraction and separation of REE in solution. Nanomaterials have become very interesting in this area because, compared to bulk material, they provide a larger specific surface area and higher surface activity (Yurchenko et al., 2012) which facilitates the possibility of surface functionalization with adequate and adsorption-efficient organic ligands.

1.1 Rare Earth Elements. Why are they so important?

REE have several industrial uses worldwide, primarily within the electronics and electrical fields. REE based materials are used in many more products than is generally imagined. Their uses and application fields are almost too numerous to list, but the major ones include high field strength magnets (Zhang et al., 2014) which are used for instance in electric motors or wind turbines, sensing (Parker and Bretonniere, 2005), electro optical devices (Jin et al., 1997), catalysis (Shibasaki and Yoshikawa, 2002), advanced batteries, phosphors for fluorescent lighting and display panels, optical fiber communications, unique materials and so on (Bünzli and Piguet, 2002). Figure 1 shows the major applications of REE and each percentage of use in respect to the total REE consumption

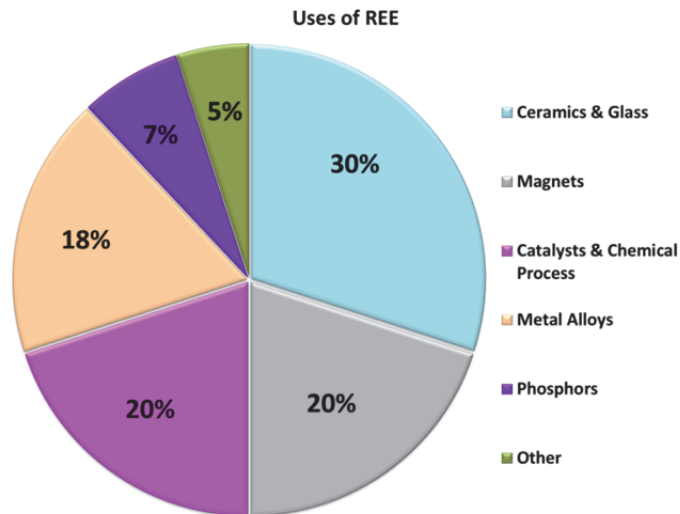


Figure 1. Uses of the Rare Earth Elements (EURARE, 2013)

In the field of Ceramics and Glass we can find applications such as polishing media, UV resistant glasses, thermal glass, capacitors, sensors, colorants, refractories, fuel cells and superconductors among others.

As for ultra strong magnets, they are applicable in motors and generators, HD drives, Microphones and Speakers, Magnetic Resonance Imaging (MRI), magnetic refrigeration and so on. Strong magnets are also needed for many defence applications, which allows to point out the importance of REE for military purposes. REE are essential for missile guidance systems, lasers, smart bombs, sonar and underwater mine detection, radar and antimissile defense, jet engines, laser range finders and targetings, electronic countermeasures and satellite communication systems.

REE are also essential for catalysts and chemical processes such as petroleum refining, automotive catalysts, diesel additives and water treatment.

Regarding metal alloys, they are used in NimH batteries, superalloys, Al-Mg alloys and steel, among others.

When it comes to Phosphors, REE are needed for LED, LASER, flat panel displays, fluorescent lamps, X-ray imaging, optical sensors and fibre optics.

Other uses of REE include such as fertilizers, pigments, nuclear applications and medical tracers (EURARE, 2013)

Taking into consideration all these applications, it seems obvious that the worldwide demand of REE has enormously increased and will continue to do so. China controls nowadays the majority of REE market and the recent establishment of strict export quotas constitutes a risk for Europe for a reliable and sufficient supply of REE. Therefore, it has become a priority to develop strategies for an economically viable and sustainable self-dependent REE industry.

1.2 Rare Earth Elements. Abundance and occurrence in nature.

Rare Earth Elements is the collective name for 17 chemically similar metallic elements that occur in a wide range of REE bearing minerals and are mined collectively. According to the IUPAC definition, “rare earth metals” (REMs, or “rare earth elements”, REEs) include the group of 15 elements starting from lanthanum (atomic no. 57) to lutetium (atomic no. 71), known as the “lanthanides”, and Scandium (atomic no. 21) and Yttrium (atomic no. 39), having similar physical and chemical properties are also included in the REE family. Based on their location in the periodic table and their atomic weights, REE can be classified in Light Rare Earth Elements (LREE) and Heavy Rare Earth Elements (HREE). Lanthanum, Cerium, Praseodymium, Neodymium, Promethium, and Samarium (atomic no. 57-62) belong to the first group (LREE), while Europium, Gadolinium, Terbium, Dysprosium, Holmium, Erbium, Thulium, Ytterbium and Lutetium (atomic no. 63-71) constitute the HREE (IUPAC, 2005). This last group of REE are generally used in high tech applications. For example, Erbium is used for fiber optics in communications, Europium and Terbium are used in phosphors and Gadolinium is used for Magnetic Resonance Imaging. All of them occur naturally in Earth, except Promethium, which is obtained by synthetic methods.

Despite their name, REE are indeed quite abundant in the earth crust, especially LREE, which are more commonly and easily extracted than HREE. The misleading term “rare earth” comes historically from the chemist Carl Axel Arrhenius (1757-1824), after he discovered them in 1784 in the dumps of Ytterby (Sweden) quarries. They were called “rare” because when they first were discovered, he thought that they were present in very small amount, and “earths” because, when forming oxides, REEs have an earthy appearance (Massari and Ruberti, 2013). But they are actually not rare at all, being most of them more abundant in earth crust than silver or gold (Hurst, 2010). For example, Cerium (6.6×10^{-3} % by weight in the Earth’s crust) has a similar abundance of that of Cu and four times higher than Pb. Even Thulium and Lutetium, which are the two least abundant REEs, are 200 times more common than gold. REE can be found in almost all massive rock formations.

REE can be found in many diverse minerals, including silicates, carbonates, oxides and phosphates. Around 270 minerals are known to contain the REE as an essential part of their crystal structure, but only a small number are ever likely to have commercial significance. The majority of historical production has come from a small number of minerals, which are mainly bastnäsite, monazite, and xenotime. Many REE enrichments are associated with other

minerals such as apatite, allanite and eudialyte, and research on the processing of these minerals is ongoing.

As it can be now understood, the problem with REE relies, not in their concentration, but in the difficulty to find economically exploitable deposits, and the fact that, due to their chemical similarities and their joint occurrence in nature, their separation becomes a very challenging and high-tech demanding process.

It is in this point where solid inorganic adsorbent materials gain importance. A special focus has been set to the development of silica (SiO₂) based nanoparticles as high performance sorbent materials (Yurchenko et al., 2012, Melnyk et al., 2012, Dudarko et al., 2008). Silica (SiO₂) is a basic raw material that is widely used in several fields such as electronics, ceramics and polymer material industries. Due to its small-diameter particles, ultrafine nanoscale silica offers many advantages for adsorption applications (Liou, 2004). In comparison with bulk material, SiO₂ NPs exhibits a much higher surface area, which facilitates the adsorption process, and furthermore they offer the possibility of being surface-functionalized with organic ligands. All these properties, on whole, provide great applicability for high binding capacity towards REE.

However, in order to make this process industrially viable and efficient, having easily removable adsorbent materials becomes an attractive asset. This, together with the magnetic nature of REE, gives rise to the idea that magnetic hybrid nanoadsorbents are a potentially suitable and effective alternative. The development of novel highly stable nanoadsorbents consisting of a magnetic core and a surface covering layer of SiO₂ seems to be an ideal solution, since the magnetic core would provide the easy removal and the interesting magnetic properties, and the SiO₂ layer would provide the already mentioned suitable characteristics for adsorption, such as the high surface area and the possibility of surface functionalization.

1.3 Magnetic Iron Oxide Nanoparticles

Magnetic nanoparticles (MNPs) possess many interesting properties which are advantageous for diverse applications in very various fields, such as catalysis (Cornell and Schwertmann, 2003, Azhar Uddin et al., 2008, Li et al., 2008, Shi et al., 2007, Zhang et al., 2007, Wang and Willey, 1998, Al-Sayari et al., 2007, Wang and Davis, 1999, Bautista et al., 2007), biomedical applications including development of immunoassays, magnetic resonance imaging contrast agents, targeted drug delivery vehicles and magnetic hyperthermia among others (Tartaj et al., 2003, Jurgons et al., 2006, Qiang et al., 2006, Xu et al., 2006, Lübbe et al., 1999, Zheng et al., 2006, Ai et al., 2005, Gonzales and Krishnan, 2005, Lee et al., 2005, Sadeghiani et al., 2005), technological applications like data storage (Reiss and Hutten, 2005) or environmental protection applications like wastewater treatment (Jiang et al., 2011, Nassar, 2010).

1.3.1 Iron oxides

Iron oxides exist in diverse forms in nature, being magnetite (Fe_3O_4), maghemite ($\gamma\text{-Fe}_2\text{O}_3$) and hematite ($\alpha\text{-Fe}_2\text{O}_3$) the most common ones (Cornell and Schwertmann, 2003).

Hematite does not exhibit magnetic properties and therefore is not interesting for our purposes, while magnetite possesses the strongest magnetism of any transition metal oxide (Cornell and Schwertmann, 2003, Majewski and Thierry, 2007). As for maghemite, its crystal structure is closely similar to that of magnetite and it forms continuous solid solutions with magnetite (Majewski, 2008).

1.3.2 Magnetic behaviour of iron oxides and MNPs

Magnetic iron oxides contain Fe (III) ions in a spinel structure occupying octahedral spaces between densely packed oxide anions. Both magnetite and maghemite follow this crystal structure and therefore both display magnetic behaviour, being magnetite the one with a stronger magnetism, as previously mentioned. These two iron oxides can be transformed one into another via redox reactions.

In a bulk ferromagnetic material, the magnetization vector M is the sum of all the magnetic moments of the atoms in the material per unit volume of the

material. The bulk material is constituted by domains, having each domain its own magnetization vector. The magnetization moments of all the domains in the material might not be aligned and this can result in a decrease in the overall magnetic properties of the material. But when the length scale becomes small, the number of domains decreases until the size of the material is below some critical size d_c , in which case there is one single domain (Teja and Koh, 2009).

A single magnetic domain has no hysteresis loop in its magnetization curve and is said to be superparamagnetic. Iron oxide nanoparticles below 20 nm often have superparamagnetic behaviour at room temperature (Cornell and Schwertmann, 2003).

Magnetite nanoparticles exhibit the most interesting magnetic properties, but they are easily transformed to maghemite by means of oxidation or temperature increases. This transformation into maghemite can result in a loss of magnetic properties, but working in nanoscale allows to still have a magnetic enough material for the required purposes.

1.3.3 MNPs as novel nanoadsorbents

In what concerns to the main focus of this work, nanoparticles feature unique characteristics providing them appropriate adsorption surfaces (Faraji et al., 2010, Xu et al., 2012). The main advantages of magnetic iron oxide nanoparticles for REE adsorption arise from their magnetism, being this a very attractive property for an adsorbent material since it allows a facile further separation from the liquid solution via application of an external magnetic field. (Shen et al., 2009). Iron oxide MNPs constitute the basis of novel nanoadsorbent materials which provide profitable characteristics such as requiring simple equipment, facile operation, high efficiency and high potential for restoration and reusability (Shahriari et al., 2014). Furthermore, they are economical for industrial upscaling and they have good stability and very low toxicity when compared with another counterpart ions (Soenen et al., 2012, Wilkinson et al., 2012). In comparison with bulk material, MNPs open more possibilities for adsorption due to the higher surface area and the potential for appropriate surface decoration depending on the desired purpose.

Despite the instability of MNP under harsh conditions such as strong acidic media, it is possible to stabilize them against leaching via deposition of a protecting layer. Synthesis of core-shell MNPs seems to be a good solution for this situation. Some sophisticated approaches involving the creation of a shell consisting of a noble metal have been made (Thanh, 2012) but they are mostly

applicable in medicine due to cost reasons. Among the diverse types of coating materials, which include noble metals, metal oxides and polymer materials, silica coating has been extensively studied and has several advantages arising from the stability under aqueous solutions, protection of the magnetic core and therefore prevention of direct contact with external agents and the enhancement of their biocompatibility, hydrophilicity and dielectric properties (Stjerndahl et al., 2008, Im et al., 2005, Lu et al., 2007a). Moreover, silica coating facilitates further surface modification of the NPs due to the silanol (-SiOH) groups on the surface. This silanol groups can be functionalized with amino, thiol and carboxyl groups among others, resulting in optimal functionalized nanomaterials for bio-labeling, drug delivery and targeting applications (Gupta and Gupta, 2005, Lu et al., 2007b).

A previous study showed that the encapsulation of the iron oxide MNPs leads to oxidation from magnetite to maghemite and consequently some loss in the magnetic characteristics, but the material remains magnetic enough for the required purposes, with a magnetic susceptibility at a level of ca. 6 emu/g, which is in good agreement with the industrial requirements for magnetic separation (Pogorilyi et al., 2014). The larger the amount of silica to be added, the longer the process will be and therefore the higher the oxidation of the original magnetite phase will be, but on the other hand, the layer of silica around the MNPs core helps to protect them for further oxidation (and therefore further transformation to maghemite phase with the consequent progressive loss of magnetic properties), so there shall be an optimization of the encapsulation process leading to a layer which is protective enough for the MNPs core but doesn't hinder their unique properties.

There are few methods known to produce core-shell silica coated MNPs, and among them, microemulsion and alkaline hydrolysis of tetraethyl ortosilicate (TEOS) have been pointed out as the major methods for core-shell NPs (Santra et al., 2001, Stöber et al., 1968). The last method, well-known as the Stöber method has proved to be a facile and effective process to synthesize uniform spherical colloidal nanoparticles. Furthermore, the reaction parameters can be adjusted and optimized, giving the possibility to tune the resulting nanoparticles for the desired purpose.

Adsorption of pollutants by iron oxide MNPs, more specifically heavy metals, has been extensively studied, including, among many others, investigations in oil refinery wastewater treatment (Rasheed et al., 2011), paper mill wastewater treatment (Zhang et al., 2011), color removal from water (Absalan et al., 2011, Iram et al., 2010), methylene blue removal from aquatic environment (Rakhshae and Panahandeh, 2011), reduction of polybrominated diphenyl ethers (Fang et al., 2011a), adsorption of cadmium from aquatic

environments (Chen et al., 2011, Tu et al., 2012), copper and chromium (VI) adsorption from aquatic environment (Shen et al., 2012), chromium (VI) removal from electroplating wastewater (Fang et al., 2011b), removal of nickel, cadmium and lead ions from water (Badruddoza et al., 2013), decontamination of medical samples (Melnyk and Zub, 2012, Mel'nik et al., 2012) and removal of chromium (III) (Shahriari et al., 2014).

However, very little has been studied about the adsorption of REE by magnetic silica adsorbents. Dudarko and co-workers have studied the adsorption of Dy^{3+} and Nd^{3+} by silica modified with phosphonic acid derivatives (Dudarko et al., 2008). This work, together with the work carried out in this thesis, show the advantages that silica based adsorbents, and more specifically magnetic silica adsorbents offer in the field of adsorption of REE, opening new possibilities for the development of novel hybrid high-efficient and selective nanoadsorbents.

2 Research objectives

This licentiate thesis constitutes a part of the PhD project which is being carried out under the frame of the European Project EURARE. EURARE aims to set the basis of an economically viable and sustainable industry of REE within Europe. Many research institutions and mining companies are involved in this project, dealing with and trying to solve many different problems and issues related with REE production.

This work is focused on the development of new hybrid magnetic nanoadsorbents, based on magnetic silica nanoparticles decorated on the surface by appropriate organic ligands with high affinity and selectivity towards REE.

In order to make it more understandable, this work can be divided in two parts:

- The first part is dedicated to the synthesis and characterization of three different suitable organic ligands for REE adsorption, their attachment into the surface of SiO₂ nanoparticles and the study of their REE uptake efficiency in the view of using them as nanoadsorbent models for the second part.
- The second part of the work focuses on the development of hybrid magnetic nanoadsorbent materials based on iron oxide MNPs and covered by a protective layer of SiO₂, decorating the surface of these NPs with the iminodiacetic acid (IDA) derived organic ligand (which was synthesized and tested in the first part of the work). In this second part, not only REE uptake efficiency was tested but also selectivity towards different types of REE (LREE or HREE) and an effort has been also put in explaining the observed selectivity at a molecular level. The developed approach has been tested on both model solutions and real industrial leachates from REE ores.

3 Experimental

3.1 Synthesis of organic ligands (Paper I)

Three different organosilane derivatives, denoted as **L1**, **L2** and **L3** were synthesized (Tarn et al., 2013, Puri et al., 2011, Claramunt et al., 2005). Ligand 1 bears an iminodiacetic acid (IDA) attached to a siloxane fragment via an urea-based group. The IDA fragment offers interesting coordination potential with REE through the carboxylic groups. On the other hand, the pyridine ring, present in the structure of L2, offers good stability towards radioactivity. This is an issue to take into considerable account when dealing with REE, since they are commonly found together with radioactive elements such as Thorium. As for L3, it is also an IDA derivate ligand, but via a more chemically stable alkyl group attachment to the imino function of IDA. Figure 2 shows the structures of the three synthesized organic reactants used for grafting of the NPs.

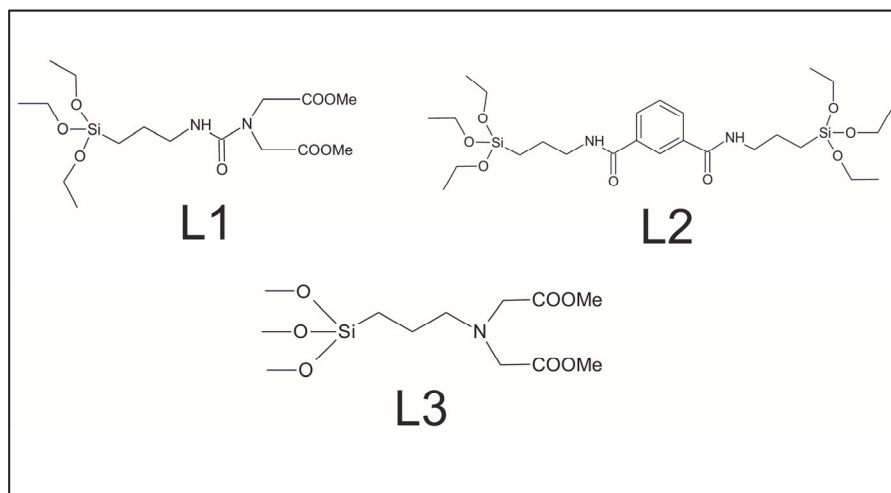


Figure 2. Chemical structures of the synthesized organosilane derivatives

L1 was synthesized from the reaction between 3-isocyanatopropyltriethoxysilane (ICPTES) and dimethyl iminodiacetate in chloroform at 80°C, under reflux and N₂ atmosphere. L2 and L3 were synthesized following procedures previously described in literature (Claramunt et al., 2005, Franville et al., 1998). L2 was synthesized from 3-iodopropyltriethoxysilane (IPTES) and dimethyl iminodiacetate in the presence of N,N-diisopropylethylamine (DIPEA) as catalyst, in toluene and under reflux and N₂ atmosphere. L3 was synthesized from 3-aminopropyltriethoxysilane (APTES) and 2,6-pyridinedicarbonyl dichloride in the presence of trimethylamine (TEA) as catalyst in dichloromethane (DCM), at room temperature and under N₂ atmosphere.

3.1.1 Synthesis of Dimethyl Iminodiacetate (starting material for L1)

IDA (1g, 7.51 mmol) was suspended in 50 mL of anhydrous methanol. Thionyl chloride (SOCl₂) (1.79g, 15.03 mmol) was added dropwise to the reaction flask and the mixture was refluxed under N₂ atmosphere for 4 hours. The mixture was then cooled to room temperature and the solvent was evaporated in a rotary evaporator, yielding a white powder which was dissolved in 5 mL of distilled water, neutralized with a solution of Na₂CO₃. Finally, extractions with ethyl acetate were carried out three times (35 mL of ethyl acetate each time) and the combined organic phases were dried over Na₂SO₄, then filtered and evaporated in the rotary evaporator, yielding a slightly yellow liquid.

3.1.2 Synthesis of L1

Dimethyl iminodiacetate (0.1 mL, 0.62 mmol) and dry chloroform (1 mL) was added to an oven dried round bottom flask. Then, ICPTES (0.15 mL, 0.62 mmol) was added dropwise to the reaction. The reaction mixture was refluxed under N₂ atmosphere for 5 hours. After this time, the solvent was evaporated in the rotary evaporator, and the obtained liquid was purified by flash column chromatography using a mixture of hexane/ethyl acetate 3:1 as eluent.

3.1.3 Synthesis of pyridine-2,6-dicarbonyl dichloride (starting material for L2)

2,6-pyridine dicarboxylic acid (500 mg, 2.99 mmol) was suspended in 30 mL of dry toluene. SOCl_2 (4.3 mL, 59.8 mmol) was added dropwise to this suspension in an ice bath. The reaction was then refluxed under N_2 atmosphere for 3 hours. After the reaction, the solvent was evaporated under reduced temperature in the rotary evaporator, yielding a white powder.

3.1.4 Synthesis of L2

Pyridine-2,6-dicarbonyl dichloride (304.5 mg, 1.49 mmol) was dissolved in 10 mL of dry DCM and added to a 50 mL three-necked round bottom flask. With the help of a pressure equalising addition funnel, DCM (5 mL), APTES (0.73 mL, 3.13 mmol), and TEA (1.1 mL, 8.22 mmol) were slowly added to the reaction mixture under N_2 atmosphere. The reaction mixture was stirred overnight at room temperature and afterwards the reaction solvent was evaporated under reduced temperature in a rotary evaporator and the reaction product was purified by flash column chromatography using a mixture of hexane/ethyl acetate/MeOH (1:1):10% as eluent.

3.1.5 Synthesis of L3

Dimethyl iminodiacetate (1 mL, 6 mmol) and IPTES (1 mL, 5 mmol) were dissolved in 5 mL of dry toluene under N_2 atmosphere. DIPEA (5 mmol) was added to the reaction mixture and refluxed overnight under N_2 atmosphere. The mixture was then cooled to room temperature and an extraction with a mixture of brine water/toluene 1:1 was carried out three times. The combined organic part was dried over Na_2SO_4 and then evaporated under reduced pressure in the rotary vapour, yielding a yellow liquid.

The synthetic routes carried out are schematized in Figure 3.

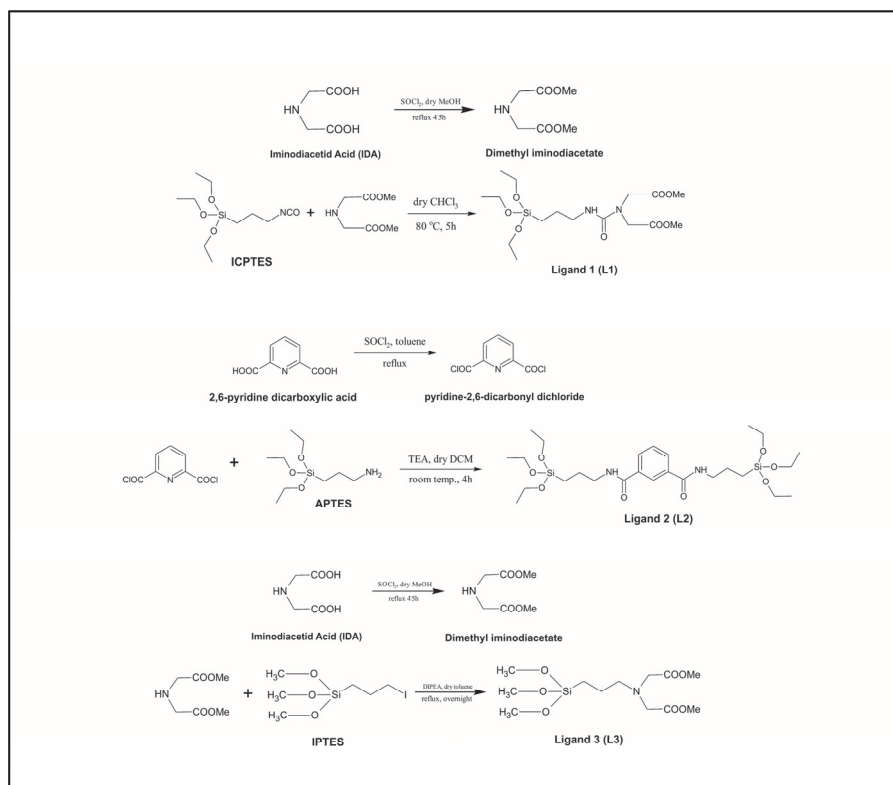


Figure 3. Synthetic pathway for the three organosilane derivatives

3.2 Synthesis of SiO₂ nanoparticles (SNPs) (Paper I)

The synthesis of SNPs was carried out following an optimized Stöber procedure (Effati and Pourabbas, 2012). Among the different synthesis methods for SNPs, Stöber synthesis (Stöber et al., 1968) has been regarded as one of the simplest and most effective methods, leading to spherical and narrow dispersed silica nanoparticles. The method allows tuning of the reaction parameters. In a typical Stöber procedure, a solution of 9.5M H₂O and 0.9M NH₄OH (25%) was prepared in 200 mL of ethanol and heated at 65°C under N₂ atmosphere. Tetraethyl ortosilicate (TEOS) (11.16 mL) was added dropwise under vigorous stirring. The reaction was stirred for 1 hour and afterwards the mixture was centrifuged at 10000 rpm for 10 minutes and washed 3 times with 20 mL of distilled H₂O and 2 times with 20 mL of ethanol. As a final step, the nanoparticles were dried under N₂ atmosphere at room temperature with the help of a Schlenk line.

3.3 Synthesis of Fe₃O₄ MNPs (Paper II)

There are several methods regarded in literature for the synthesis of magnetic nanoparticles, such as microemulsion (Chin and Yaacob, 2007), sol-gel synthesis (Albornoz and Jacobo, 2006), sonochemical reactions (Hee Kim et al., 2005), hydrothermal reactions (Wan et al., 2005), hydrolysis and thermolysis of precursors (Kimata et al., 2003), flow injection (Salazar-Alvarez et al., 2006), electrospray synthesis (Basak et al., 2007) and obtaining as by-product in the synthesis of alkali iodides (Pogorilyi et al., 2014). However, the most common method for preparation of magnetite MNPs is probably the chemical coprecipitation of iron salts (Martínez-Mera et al., 2007, Qiu et al., 2005). This technique is probably the simplest and most efficient chemical pathway to obtain MNPs. Iron oxides are generally prepared by addition of a strong base to a stoichiometric mixture of ferrous and ferric salts in aqueous medium.

In this work, MNPs were prepared by co-precipitation from a stoichiometric solution of iron (II) and iron (III) chlorides with ammonia in N₂ atmosphere.

3.4 Synthesis of SiO₂ coated γ -Fe₂O₃ core-shell MNPs (Paper II)

A modified Stöber procedure previously reported in literature (Abbas et al., 2014) was followed in this case for the encapsulation of Fe₃O₄ MNPs into a protective layer of SiO₂, creating highly stable core-shell NPs. For this, 100mg of the previously synthesized Fe₃O₄ MNPs were dispersed in 32 mL of miliQ water and sonicated for 20 minutes. Then, this dispersed solution was mixed with 160mL of ethanol while slowly adding 4 mL of NH₄OH 25%. After this, 1.6 mL of TEOS were added dropwise, achieving a SiO₂:FeO_x molar ratio of 6:1. This mixture was stirred for 20 hours and after that, the core-shell γ -Fe₂O₃@SiO₂ NPs were separated from the solution via magnet. They were washed three times with 25 mL of distilled H₂O and twice with 25 mL of ethanol and dried under N₂ atmosphere.

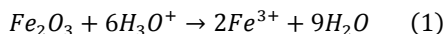
3.5 Synthesis of organic ligand grafted SiO₂ NPs and organic ligand grafted core-shell γ -Fe₂O₃@SiO₂ MNPs (Paper I & II).

100 mg of SiO₂ NPs were dispersed in 10 mL of dry toluene. To this dispersion, the organic reagents L1, L2 and L3 were added (0.06 mmol). The reaction mixture was refluxed overnight under N₂ atmosphere. The resulting hybrid NPs were centrifuged at 10000 rpm for 10 minutes and washed 3 times with 20 mL of toluene and twice with 20 mL of ethanol. Finally, the NPs were dried under N₂ atmosphere in the Schlenk line.

For the core-shell γ -Fe₂O₃@SiO₂ NPs a similar procedure was followed, but only with L3 as it showed to be the most efficient for REE uptake according to the investigations carried out in Paper I. In this case, 1.2 g of γ -Fe₂O₃@SiO₂ were dispersed in 20 mL of anhydrous toluene. To this dispersion, L3 (100 mg, 0.62 mmol) was added. The reaction mixture was refluxed overnight under N₂ atmosphere. After the reaction, the ligand grafted γ -Fe₂O₃@SiO₂ NPs were washed for 3 times with 25 mL of toluene and twice with 25 mL of ethanol. As a last step, the NPs were dried under N₂ atmosphere in the Schlenk line.

3.6 Leaching test over acidic media of γ -Fe₂O₃@SiO₂ NPs

It is very important for industrial purposes that the synthesized core-shell iron oxide MNPs are resistant under acidic conditions for the repetition of the RE separation. The release of RE is usually carried out in acidic media, so it is necessary to achieve highly stable particles. Therefore, leaching tests for γ -Fe₂O₃@SiO₂ NPs were carried out with a solution of 0.1M HNO₃ containing 0.5% of KSCN. When Fe³⁺ is released to the solution in acid media, it would form a complex with thiocyanate and therefore give a red coloration to the solution which would be proof of Fe³⁺ leaching from the particles (equations 1 and 2).



3.7 Synthesis of molecular model compounds (IDA-RE³⁺) (Paper II)

100 mg of IDA (0.75 mmol) were dissolved in 5 mL of distilled H₂O. To this solution, 0.75 mmol of RE(NO₃)₃ were added and stirred overnight. The resulting solution was left for crystallization in open air for a week. The concentration of solutions by evaporation produced syrup-like media from which some clashes of needle-shaped crystals were slowly formed on further drying.

3.8 REE uptake and release studies on ligand grafted SiO₂ and γ -Fe₂O₃@SiO₂ NPs (Paper I & II)

3.8.1 Static adsorption studies

As stock solutions, 0.025M RE(NO₃)₃ solutions were prepared (RE = Dy, Nd for SiO₂ NPs; RE = Dy, Nd, La, for γ -Fe₂O₃@SiO₂ NPs). To 50 mg of organic ligand NPs (either SiO₂ NPs or γ -Fe₂O₃@SiO₂ NPs), a calculated amount of Ln(NO₃)₃ (corresponding to twice the quantity of matter of the ligand grafted to the surface of the NPs –according to TGA results-) was added. NaNO₃ 1M was added up to a final concentration of 0.1M in a total volume of 20 mL, which was completed with miliQ water. The mixtures were then sonicated for a couple of minutes in order to disperse the NPs in the solution and they were left in static conditions for different times (2, 8, 24 and 48 hours). After the corresponding time, the mixtures were centrifuged at 10000 rpm for 10 minutes in the case of SiO₂ NPs. In the case of γ -Fe₂O₃@SiO₂ NPs, the NPs were separated from the solution via magnet. The NPs were washed once with 20 mL of distilled water and both the first and the washing solutions were collected in an Erlenmeyer and the solid sorbent was dried under N₂ atmosphere at room temperature.

In the case of γ -Fe₂O₃@SiO₂ MNPs, also binary mixtures of REE (La-Dy and Nd-Dy) in a molar ratio of 1:1 were tested for selectivity studies.

3.8.2 Dynamic adsorption studies

The same procedure as explained in 3.6.1 was followed, with the only difference that the mixtures containing the NPs and the REE salts were mixed in an orbital shaker at 130 rpm for different times (2, 8, 24 and 48 hours).

3.8.3 Desorption studies

30 mg of NPs bearing trivalent RE cations adsorbed according the procedure above explained, were put in contact with 5 mL of HCl 1M and 15 mL of miliQ water, resulting in a mixture with a pH=1. This mixture was shaken on the orbital shaker at 130 rpm for 24 hours, and the particles were separated from the solution via centrifugation (10000 rpm during 10 min) or via magnet depending on whether we were working with magnetic or non-magnetic NPs. The collected solutions needed to be neutralized in order to be able to perform complexometric titrations on them, so evaporation and redilution with distilled water was carried out until pH= 6.

3.8.4 Complexometric titrations of RE (Dy^{3+} , Nd^{3+} , La^{3+}) in mother liquor over organic ligand-grafted NPs

The collected solutions in the adsorption studies were titrated with EDTA tetrasodium salt 5 mM using xylenol orange as indicator. EDTA complexates with RE trivalent cations in a 1:1 ratio, therefore the amount of RE cations adsorbed to the surface of the NPs can be calculated by subtraction, since the initial amount put in contact with the NPs was a known amount, and the remaining amount in solution is what is determined by titration. Xylenol orange is an organic reagent, frequently used as a tetrasodium salt as an indicator for metal titrations. It appears red in the titrand and yellow once the titration reaches its endpoint. Its optimum working pH is around 5.5.

3.9 Materials characterization

Several techniques have been used in order to check the purity of the synthesized organic ligands, their effective grafting onto the surface of the NPs, the morphology of the adsorbents and their uptake and release capacity towards REE.

3.9.1 Solution ^1H -NMR and ^{13}C -NMR for the organic reactants (Paper I)

Solution ^1H -NMR and ^{13}C -NMR spectra of the organic reactants and the intermediates were recorded on a Bruker Avance spectrometer, operating at 600 MHz in the case of ^1H -NMR and 150 MHz in the case of ^{13}C -NMR. CDCl_3 was used as solvent and tetramethylsilane (TMS) as internal standard. The spectra were recorded at 25°C , coupling constants (J values) are given in Hz and chemical shifts are given in parts per million (ppm).

3.9.2 Solid state ^{29}Si and ^{13}C NMR for the ligand grafted SiO_2 NPs (Paper I)

Solid state NMR analysis was performed in order to confirm the grafting of the organic ligand onto the surface of the NPs. For technical reasons, the analysis was carried out only on non-magnetic SiO_2 NPs and the obtained results were taken as models for the studies carried out in paper II. These analyses were carried out at the Aveiro Institute of Materials, CICECO, at the University of Aveiro (Portugal). The solid state $^{29}\text{Si}\{^1\text{H}\}$ magic-angle spinning (MAS) cross-polarization (CP) NMR and the $^{13}\text{C}\{^1\text{H}\}$ CP/MAS NMR spectra were recorded on a Bruker Avance III 400 (9.4 T) spectrometer at 79.49 and 100.62 MHz respectively. $^{29}\text{Si}\{^1\text{H}\}$ MAS NMR spectra were recorded with $2.8\mu\text{s}$ ^1H 90° pulses, a contact time of 8 ms and a recycle delay of 5 s. The spinning rate was 9.0 kHz and high-power ^1H decoupling was applied during acquisition. The details of the followed method for this work were previously reported in the literature (Pines et al., 1973). Chemical shifts are given in ppm from tetramethylsilane (TMS).

3.9.3 Nitrogen sorption for Specific Surface Area (SSA) analysis (Paper I)

Specific surface area of the synthesized SiO₂ NPs was measured using nitrogen sorption at 77 K on a Quantachrome Autosorb I apparatus at the ENSCCF, Institute de Chimie in Clermont University, Clermont-Ferrand, France. The linear portion ($P/P_0 = 0.05-0.3$) of the Brunauer-Emmet-Teller (BET) model (Brunauer et al., 1938) was used for the calculation of SSA. Microporous surface area was estimated by the t-plot method.

3.9.4 Thermal analysis (Paper I & II)

Thermogravimetric analysis (TGA) was used in order to determine the amount of organic ligand chemically grafted onto the surface of the NPs. The analysis was carried out using a Perkin-Elmer Pyris 1 Instrument under oxygen atmosphere at a heating rate of 5°C/min in the interval of 25-600 °C.

3.9.5 Particle size distribution and surface charge analysis (Paper I)

The particle size distribution in solution was determined by nanoparticle tracking analysis, which is based on the Brownian motion of SiO₂ and ligand grafted SiO₂ NPs in solution. The measurements were carried out in a NanoSight 300 instrument.

Surface charge of SiO₂ and ligand grafted SiO₂ NPs was evaluated by ζ -potential measurements, performed in a Malvern ZetaSizer instrument at pH= 6.5.

3.9.6 Photoluminescence studies of ligand grafted SiO₂ NPs bearing RE trivalent cations (Paper I)

Photoluminescence (PL) of the nanoadsorbents after adsorption of RE constitutes a proof of adsorption, and therefore PL was studied on the organic ligand grafted SiO₂ NPs after adsorption of RE in solution. The measurements were carried out at the National Institute for Laser, Plasma and Radiation Physics in Bucharest, Romania, using a Fluoromax 4 spectrofluorimeter (Horiba) operating in both fluorescence and phosphorescence modes. The repetition rate of the xenon flash lamp was 25 Hz and the integration window varied between 0.1 and 0.5 s. The slits were varied from 5 to 29 nm

for excitation and from 1 to 5 nm for emission measurements. Time Resolved Emission Spectra (TRES) were recorded at 300 K using a tunable wavelength (from 210 to 2300 nm). The excitation light source was a NT340 Series EKSPLA OPO (Optical Parametric Oscillator) operated at 10 Hz and the detection system consisted on an intensified CCD (iCCD) camera (Andor Technology) coupled to a spectrograph (Shamrock 303i, Andor). TRES were collected using the car box technique. The gain of the micro-channel plate (MCP) varied from 30 to 100, depending on the intensity of the luminescence. PL was detected in the spectral range of $400 \text{ nm} < \lambda_{\text{em}} < 900 \text{ nm}$ with a spectral resolution varying from 0.05 to 0.88 nm. The delay after the pulse varied from 1 to 500 μs , and 100 to 300 accumulations per laser pulse were used depending on the signal to noise ratio. The near-infrared emission experiments had a setup consisting on a Jarell-Ash monochromator, S1 photomultipliers, Ge photodiodes and a Lock-in amplifier on line with a computer and excited with an OPO Rainbow-VIR/S laser at 592 nm.

3.9.7 IR spectroscopy (Paper I & II)

The surface of the nanoadsorbents was studied by Fourier-transform infrared (FTIR) spectroscopy, which provides information about the chemical bonds in the surface of the material and therefore, together with solid state NMR, is a powerful technique for confirming the efficient grafting of the organic ligands onto the surface of the NPs. The spectra were recorded as KBr pellets on a Perkin-Elmer Spectrum 100 instrument.

3.9.8 SEM and TEM microscopy (Paper I & II)

Surface morphology of the produced nanomaterials was studied by Scanning Electron Microscopy (SEM) and Transmission Electron Microscopy (TEM). For the nanoadsorbents after adsorption of RE, the surface composition was analysed by Energy Dispersive Spectroscopy (EDS) coupled to the SEM instrument.

TEM analyses were performed with a JEOL brand JEM 2100F model transmission electron microscope operating at 200 kV. The samples (about 1mg/mL) were prepared in an ethanol solution, dropped onto a carbon-copper grid and dried at room temperature.

SEM-EDS studies were carried out in a Hitachi TM-1000- μ -DEX scanning electron microscope. For each sample, 9 different points were measured by EDS in area mode, at x500, x5000 and x10000 magnification, from which the average value was calculated and reported as relative content of elements.

3.9.9 X-ray diffraction (Paper I & II)

X-ray powder diffraction (XRD) experiments were carried out with a multipurpose Bruker SMART Apex II-Instrument. The background subtraction and the identification of the patterns were made using Bruker EVA-12 program.

Data collection for single crystal of the molecular model compounds (IDA-RE³⁺) was carried out at room temperature using MoK α radiation ($\lambda = 0.71073 \text{ \AA}$) with a Bruker SMART Apex-II CCD Diffractometer. The structures were solved by direct methods. The positions of metal atoms were identified from the initial solution and all other non-hydrogen atoms were located in difference Fourier syntheses. All non-hydrogen atoms were refined first in isotropic and then in anisotropic approximation. Positions of the hydrogen atoms were calculated geometrically for the NH₂⁺ groups and CH₂- fragments, while the hydrogen atoms and the oxygen atoms of the water molecules were found in difference Fourier syntheses.

4 Results and Discussion

4.1 Solution $^1\text{H-NMR}$ and $^{13}\text{C-NMR}$ for the organic ligands and the intermediates (Paper I)

One of the main objectives of Paper I was to successfully synthesize hybrid nanoadsorbents consisting on SiO_2 NPs grafted with three different organosilane derivates. These non-magnetic hybrid nanoadsorbents would be used as models for adsorption for the studies carried out in Paper II with magnetic nanoadsorbents.

Therefore, one of the most important first steps was the synthesis of the organic reactants for grafting of the ligands and for that, $^1\text{H-NMR}$ and $^{13}\text{C-NMR}$ of the obtained products constituted a powerful technique in order to confirm the efficiency and purity of the synthesis. These analyses were carried out for the final products but also for the synthesized intermediates, in order to make sure that the final reaction was performed under the best possible conditions. Figures 4 to 8 show the $^1\text{H-NMR}$ and $^{13}\text{C-NMR}$ spectra of the synthesized compounds. The corresponding molecule structure is plotted in each spectrum, with the characteristic chemical shift of each proton/carbon.

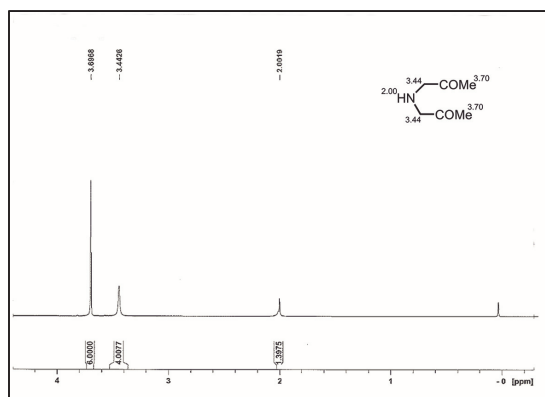


Figure 4. $^1\text{H-NMR}$ of Dimethyl iminodiacetate (600 MHz, CDCl_3)

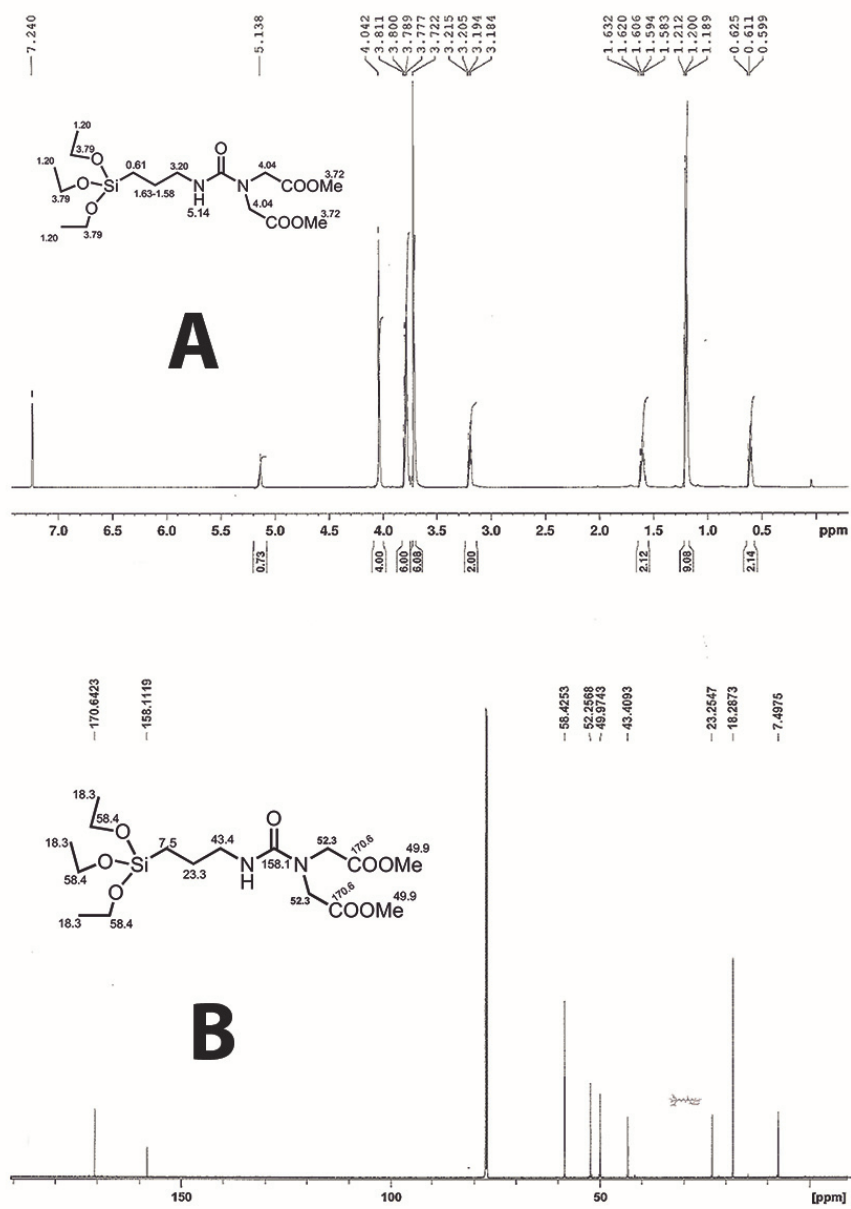


Figure 5. ^1H -NMR (A) and ^{13}C -NMR (B) of Ligand1 (600 MHz, CDCl_3)

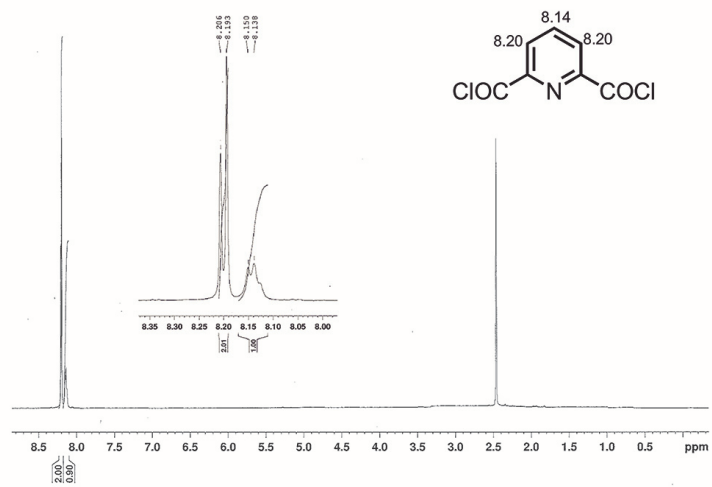


Figure 6. $^1\text{H-NMR}$ of pyridine-2,6-dicarbonyl dichloride (600 MHz, CDCl_3)

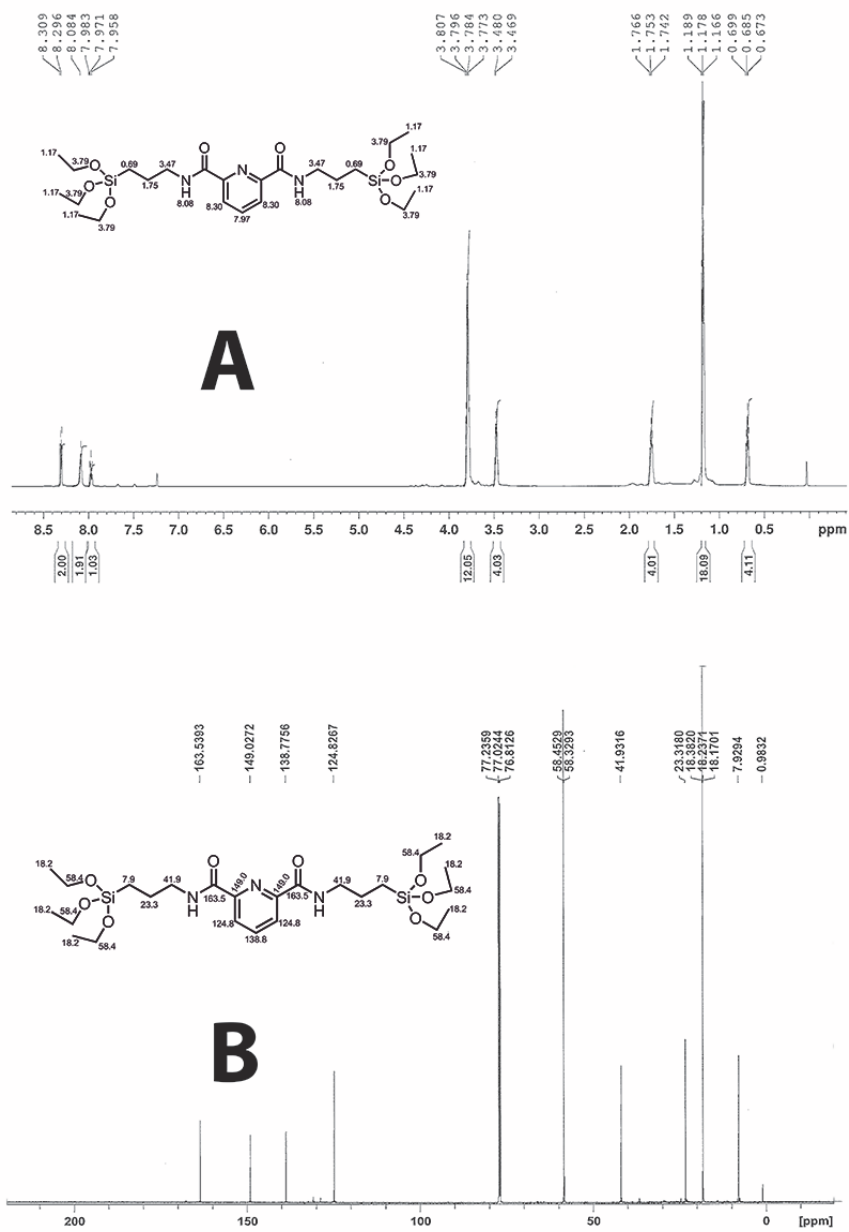


Figure 7. ^1H -NMR (A) and ^{13}C -NMR (B) of Ligand 2 (600 MHz, CDCl_3)

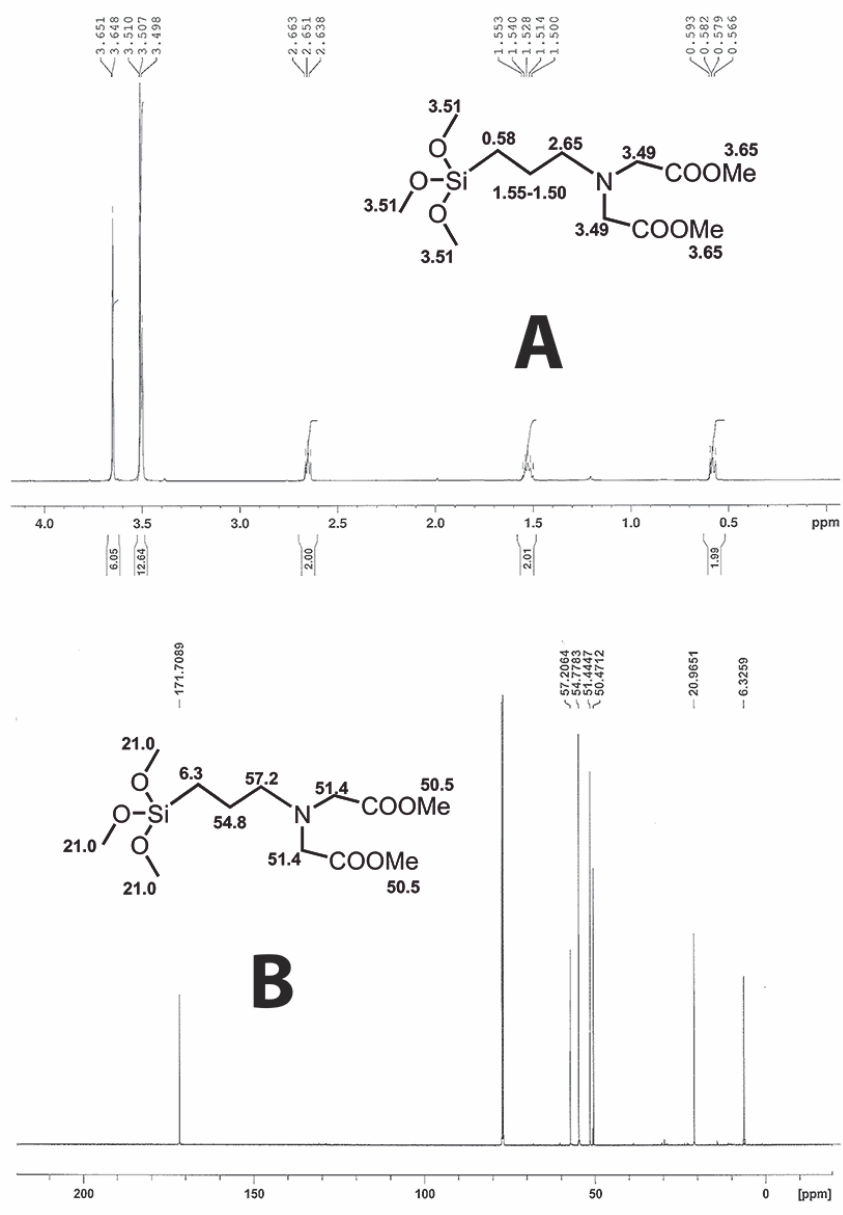


Figure 8. ¹H-NMR (A) and ¹³C-NMR (B) of Ligand 3 (600 MHz, CDCl₃)

4.2 Confirmation of ligand grafting onto the surface of the NPs

4.2.1 Solid state ^{29}Si and ^{13}C NMR for ligand grafted SiO_2 NPs (Paper I)

The functionalization of SiO_2 NPs has been confirmed by solid-state ^{13}C and ^{29}Si cross-polarization magic-angle spinning (CP-MAS) NMR (Fig.9).

Regarding ^{13}C -NMR spectra, for the NPs functionalized with L1, there are two characteristic signals attributed to carbonyl (C=O) groups. The first one, at 170.9 ppm (marked as **d** in Fig 9) corresponds to the urea group, and the second one, found at 159.2 ppm (**f**) is assigned to the ester group. All of the other remaining peaks ranging from 50.8 to 8.3 ppm are attributed to aliphatic carbons. It is important to note that the ester methyl groups from L1 and L3 were apparently removed in the process of functionalization, leaving the iminodiacetic acid functions unprotected and able to bind to the RE^{3+} cations.

The NPs functionalized with L2 possess a characteristic carbonyl group which resonates at 164.3 ppm (**d**) and the rest of the obtained peaks correspond to the alkyl chain carbons.

For L3 grafted SiO_2 NPs, the characteristic carbonyl peak can be observed at 171.9 ppm (**e**).

It can be observed in all spectra that despite the thorough washing of the NPs, there is still quite a lot of ethanol remaining, but the results are in good agreement with the expected effective grafting of the NPs surface.

Regarding the ^{29}Si CP-MAS NMR spectra, the three studied materials present several peaks which can be assigned to Q_n and T_n local environments, respectively, $\text{Si}(\text{OH})_{(4-n)}$, $(\text{OSi})_n$ and $\text{RSi}(\text{OH})_{(3-n)}(\text{OSi})_n$ (Fig 10) (Peng et al., 2005, Sharma and Sharma, 2014)

The peaks at -102 and -110 ppm are assigned to the silica network (Q_3 and Q_4 respectively). A weak shoulder at ca. -92 ppm which indicates the presence of some Q_2 environments can be observed. For the NPs functionalized with L2, resonances at ca. -68 and 56 ppm can be also observed, the latter one exhibiting a shoulder at ca. -49 ppm, which are assigned to T_3 , T_2 and T_1 sites respectively. The NPs functionalized with L3 present some weaker T_3 and T_2 peaks, while for the L1 grafted SiO_2 NPs, only some raised background can be observed in the T_3 region.

These results provide strong proof of the effective chemical bonding of the synthesized organic ligand with the surface of the SiO_2 NPs.

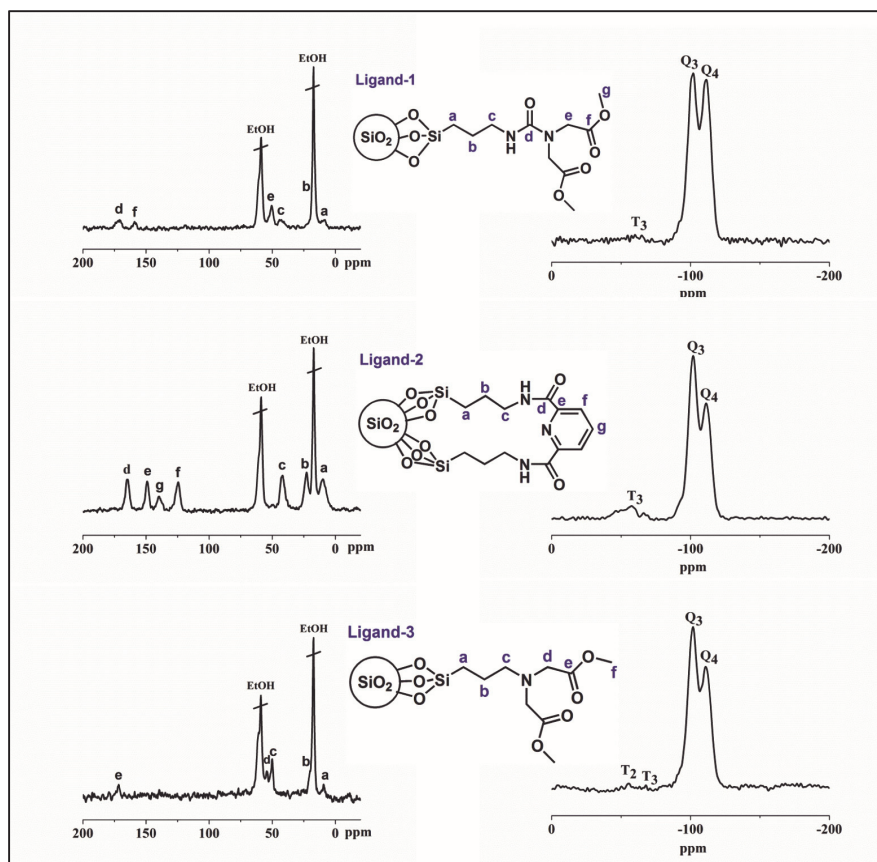


Figure 9. ^{13}C CP-MAS NMR and ^{29}Si CP-MAS NMR spectra of the functionalized SiO_2 NPs.

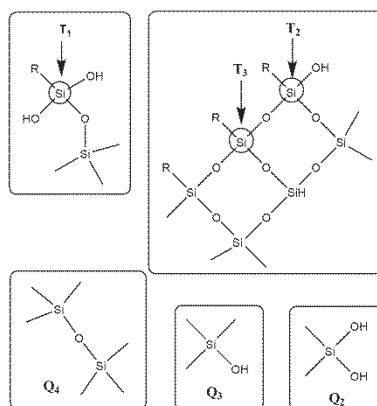


Figure 10. Q_n type (Q_4 , Q_3 , Q_2) and T_n type (T_3 , T_2 , T_1) Si local environments

4.2.2 FTIR spectroscopy (Paper I & II)

FTIR spectroscopy was also used as a powerful tool to confirm the grafting of the organic ligands to the surface of the NPs, since FTIR provides information about the chemical bonds in the surface.

Ligand grafted SiO₂ NPs (Paper I)

The FTIR spectra (Fig. 11) of the pure SiO₂ NPs show several characteristic peaks. The peak found at 1100 cm⁻¹ (which is saturated in order to permit better resolution) corresponds to asymmetric stretching vibration of Si-O-Si. The peaks observed at 956, 800 and 464 cm⁻¹ belong to stretching vibration of Si-OH, symmetric stretching vibration of Si-O-Si and bending vibration of Si-O-Si, respectively. The peaks at 3300 and 1635 cm⁻¹ are attributed, respectively, to the stretching and bending absorption by water and hydroxyl groups (Silverstein RM, 1981).

Agreeing with the expectations, when organic ligands were grafted onto the surface of SiO₂ NPs, new peaks could be observed in the spectra. For instance, in the spectrum A1, two stretching vibrations of the carbonyl group appeared at 1702 and 1635 cm⁻¹. The peak at 1448 cm⁻¹ is attributed to bending vibrations of the NH group present in the molecule of Ligand 1. When lanthanides are complexed with this nanoadsorbent (blue and pink lines), it can be observed that the two carbonyl stretching frequencies are shifted to lower wavenumbers, at 1697 and 1629 cm⁻¹.

In B1 spectrum, the characteristic peaks of the molecule of Ligand 2 can be identified. The peaks found at 1664, 1546 and 1448 cm⁻¹ correspond to vibrations of $\nu(\text{C}=\text{O})$, $\nu(\text{C}=\text{C})$ bonds in the pyridine ring and $\delta(\text{C}-\text{N}-\text{H})$ group, respectively. After complexation with lanthanides (spectrum B2), again it can be observed that the frequency of C=O stretching was shifted to lower frequencies.

In C1 spectrum, we can observe the stretching frequency of the carbonyl fragment of the ester group, characteristic of the ligand 3 molecule, at 1748 cm⁻¹, whereas when complexation with lanthanides occurs, this vibration is shifted to lower frequencies.

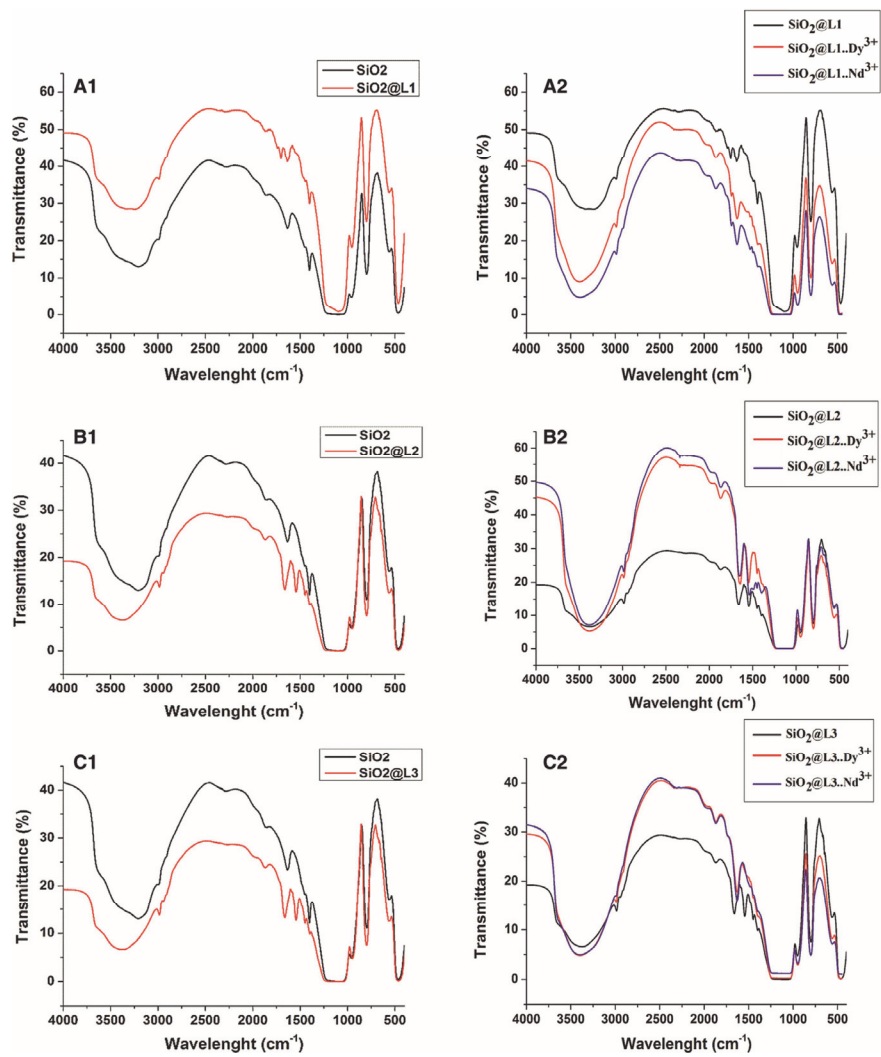


Figure 11. FTIR spectra of the synthesized ligand grafted nanoparticles. Comparison between pure SiO₂ NPs and ligand-grafted NPs (left) and comparison between ligand-grafted NPs with and without adsorbed lanthanides (right).

The surface of magnetic $\gamma\text{-Fe}_2\text{O}_3@\text{SiO}_2$ NPs was functionalized with organic ligand 3 (IDA-derivate ligand) and FTIR was used to confirm the efficient grafting (Fig. 12). A strong absorption band at 578 cm^{-1} which belongs to a characteristic band of Fe-O stretching vibrations in FeO_x NPs can be observed. The bands observed at 3400 and 1635 cm^{-1} can be attributed to the stretching and bending vibrations of the O-H bond coming from the residual water in the sample. After covering the NPs with a protective layer of silica, some characteristic bands, such as asymmetric stretching vibration of Si-O-Si, stretching vibration of Si-OH, symmetric stretching vibration of Si-O-Si and bending vibration of Si-O-Si appeared at 1096 , 956 , 800 and 464 cm^{-1} respectively.

Fe-O stretching vibration band is shifted to lower frequencies (562 cm^{-1}) after surface functionalization with ligand 3, and new bands appeared at 1733 cm^{-1} , which belongs to the C=O fragment of the carboxylic group, proving the covalent bond between the organic ligand and the surface of the NPs.

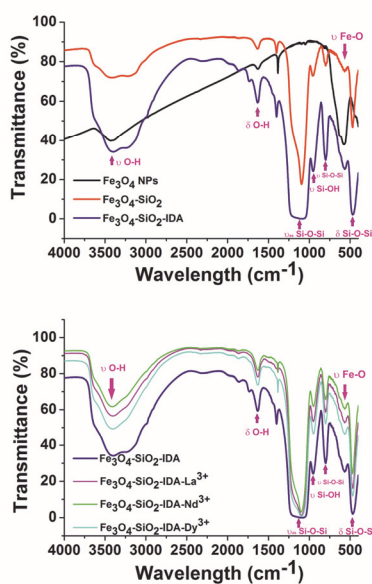


Figure 12. FTIR spectra of the Fe_3O_4 , $\gamma\text{-Fe}_2\text{O}_3\text{-SiO}_2$, $\gamma\text{-Fe}_2\text{O}_3\text{-SiO}_2\text{-IDA}$ (above) and $\gamma\text{-Fe}_2\text{O}_3\text{-SiO}_2\text{-RE}^{3+}$ in comparison with $\gamma\text{-Fe}_2\text{O}_3\text{-SiO}_2\text{-IDA}$ NPs (below)

4.2.3 Thermo-gravimetric analysis (TGA) (Paper I & II)

Ligand grafted SiO₂ NPs

Thermo-gravimetric analysis was performed on all the synthesized nanoadsorbent as another confirming technique of the surface functionalization but as well as a quantitative technique in order to determine the amount of organic ligand grafted onto the surface. The analyses were performed in the range from 25 to 600 °C. Thermal curves for L1, L2 and L3 grafted SiO₂ NPs are shown in Figure 13. The presence of water and alcohol molecules adsorbed is visible in all three samples, which leads to a loss of around 5.2 to 6% in the range of 20 to 200 °C. Between 200 and 600 °C, the molecules of L1, L2 and L3 were decomposed (with a maximal decomposition speed at around 400 °C for all of them). The weight loss in this range was 6.41, 9.16 and 6.78% for L1, L2 and L3 respectively.

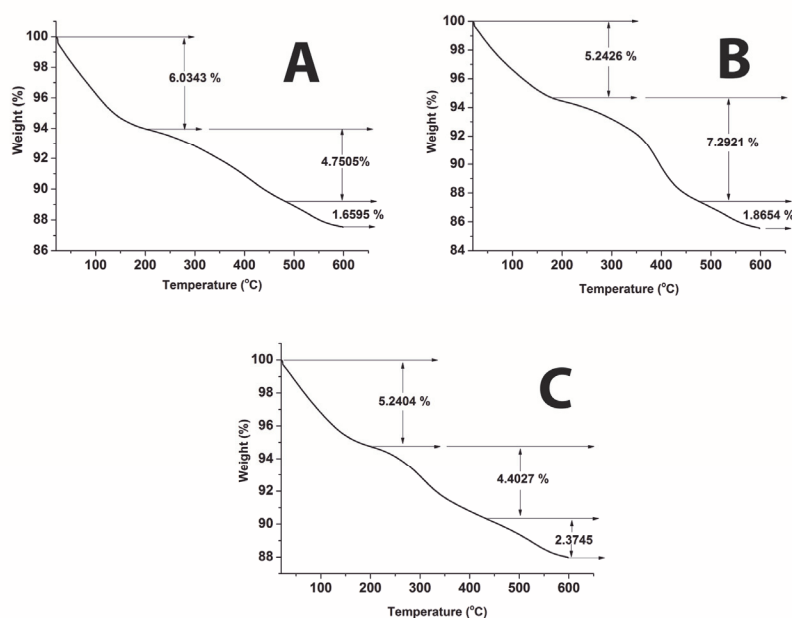


Figure 13. TGA curves of SiO₂-L1 (a), SiO₂-L2 (b), and SiO₂-L3 (c) NPs

Ligand grafted magnetic γ -Fe₂O₃@SiO₂ MNPs (Paper II)

TGA curve (Fig 14) shows that the mass loss occurs in three major steps: A first step probably related to the evaporation of surface adsorbed solvents (water, ethanol and toluene) can be observed in the range from 25 to 150 °C and leads to a loss of 5.2%. The second decomposition step occurs in the interval from 220 °C to 400 °C after a plateau where the material is thermally stable. This second step produces a weigh loss of 4.4% and it's associated with the thermal destruction of the ligand. The weight loss continues slowly after this second step with an additional release of a 1.2%, which most likely corresponds to the cracking of the residual surface alkyl siloxane species (Gonzaga et al., 2009)

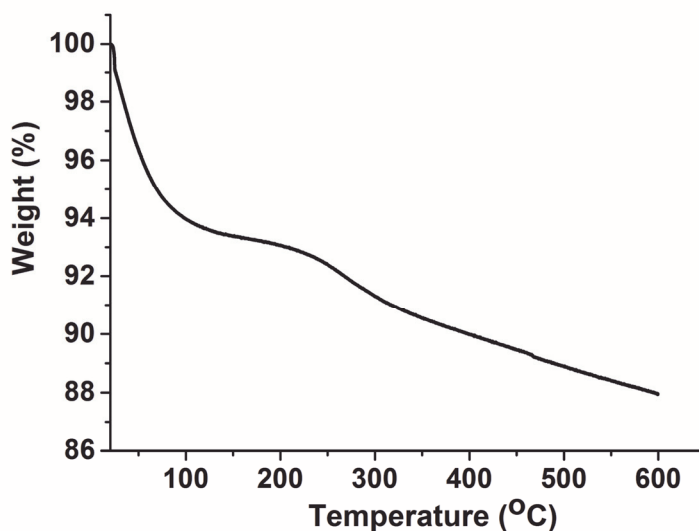


Figure 14. TGA curve for γ -Fe₂O₃-SiO₂-L3 NPs

4.3 Surface morphology and composition (SEM and TEM microscopy) (Paper I & II)

4.3.1 SiO₂ NPs and ligand grafted SiO₂ NPs (Paper I)

Stöber method, which was used in this work to synthesize spherical SiO₂ NPs, allows tuning the reaction parameters in order to vary the final particle size. For our purposes, it was important to have small particles, since they lead to a material with a higher surface area and therefore possibility to bind a higher amount of organic ligand onto the surface. Several attempts with different solution concentrations and different temperatures were made in order to control the size of the final material. The aim was to obtain particles below 100 nm but not smaller than 60 nm since a smaller size would make luminescence detection more difficult.

Table 1 shows the different synthesis conditions performed and the average particle size of the final material. As it can be seen, *method II* leads to SiO₂ NPs with an average diameter of 75 nm, which is perfectly suitable for our purposes.

No	H ₂ O	EtOH	[NH ₄ OH]	[TEOS]	Temp.	Hour	Part.Size
<i>I</i>	-	40mL	6.75 M	0.29 M	25°C	2	600 nm
<i>II</i>	9.5M	200mL	0.5 M	0.25 M	65°C	1	75 nm

Table 1. Different experimental conditions for the synthesis of SiO₂ NPs and final average size

Fig 15. shows the SEM image (x10000 magnification) of the SiO₂ particles synthesized by Method I, while in Fig. 16, the HR-TEM images of SiO₂ NPs prepared via the method II can be observed in A,C, E and F. The histograms in B and D show the size distribution of SiO₂ NPs calculated from the images A and C. Both histograms are coherent and show that the obtained particles are monodisperse and with an average diameter of 75 nm (\pm 15 nm).

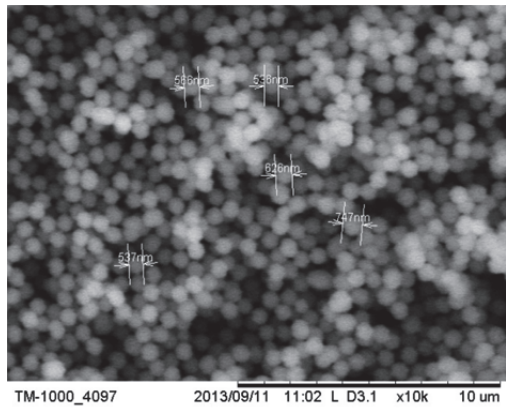


Figure 15. SEM image (magnification x10000) of SiO₂ particles synthesized via Method I

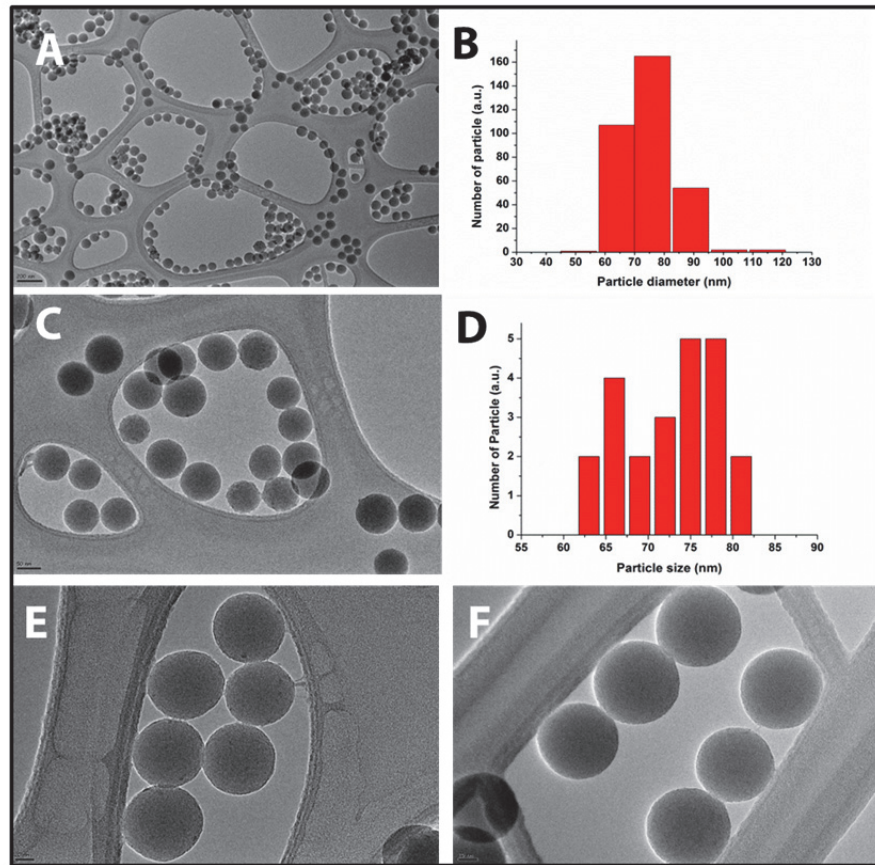


Figure 16. HR-TEM images of SiO₂ NPs (A, C, E and F) and particle size distribution histograms (B and D)

After adsorption of RE^{3+} cations by ligand grafted SiO_2 NPs, the morphology of the materials was studied by SEM (Figure 17), showing that they conserve their uniformity even on the micrometer scale.

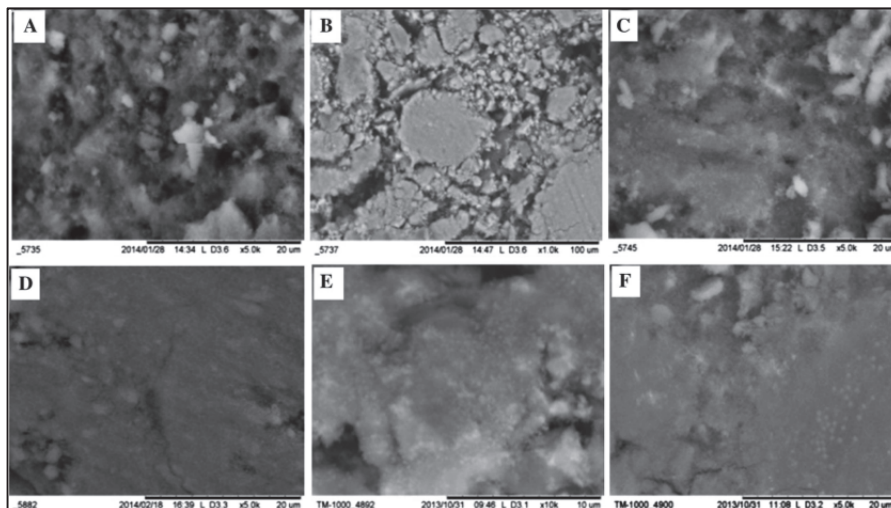


Figure 17. SEM images of a) $\text{SiO}_2\text{-L1-Dy}^{3+}$ b) $\text{SiO}_2\text{-L2-Dy}^{3+}$, c) $\text{SiO}_2\text{-L3-Dy}^{3+}$, d) $\text{SiO}_2\text{-L1-Nd}^{3+}$ e) $\text{SiO}_2\text{-L2-Nd}^{3+}$ f) $\text{SiO}_2\text{-L3-Nd}^{3+}$

4.3.2 Ligand grafted magnetic γ -Fe₂O₃@SiO₂ MNPs (Paper II)

In this case, as in the synthesis of SiO₂ NPs, two different reaction conditions were tested in order to achieve core-shell NPs with an optimal size for adsorption purposes. These two experimental conditions are shown in Table 2.

No	Fe ₃ O ₄ (mmol)	H ₂ O (mL)	Ethanol (mL)	NH ₄ OH (mmol)	TEOS (mmol)	Hours (h.)	Particle Size (nm)
I	0.4	-	40	270	11.8	2	800
II	0.4	32	160	53.4	7.0	20	100

Table 2. Reaction parameters for the synthesis of γ -Fe₂O₃-SiO₂ NPs and the obtained average final size

Figure 18A shows the HR-TEM images of the NPs synthesized under method II conditions, showing particles with an average diameter of 100 nm (\pm 15 nm). These images also show the uniform coating achieved with Stober method, with the formation of a silica layer of approximately 25 nm (Fig. 18B). The fringes can easily be seen at higher resolution (Fig. 18C) and indicate a crystalline form of iron oxide with cubic spinel structure. Fig 18D shows the mapping of Fe (green) and Si (red) elements, revealing that the silica layer emerges around aggregates of iron oxide nanoparticles.

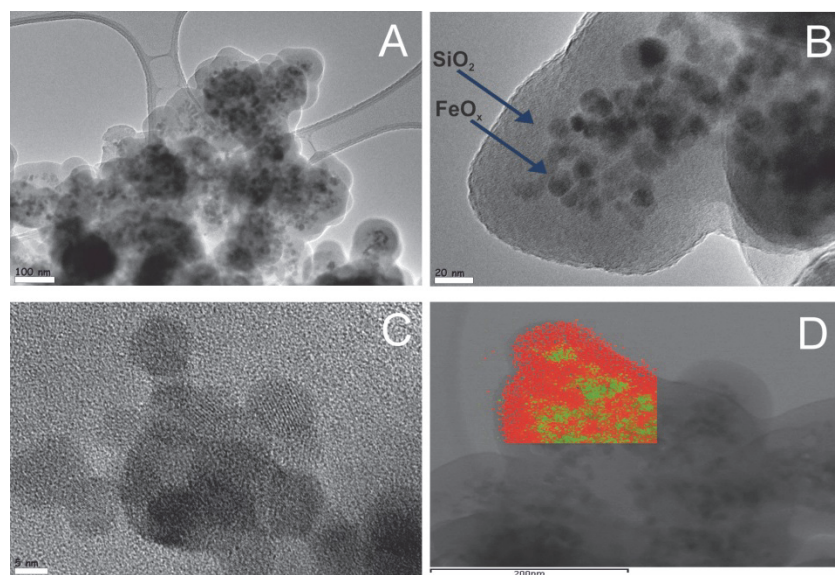


Figure 18. HR-TEM images of γ -Fe₂O₃-SiO₂ NPs (scale bar: 100, 20 and 5 nm for A, B and C respectively). Image D shows the EF-TEM mapping

4.4 Stability of γ -Fe₂O₃-SiO₂ NPs. Leaching test (Paper II)

In order to confirm the stability of the synthesized core-shell NPs under acidic conditions, a simple leaching test with a solution of HNO₃ 0.1M containing a 0.5% of KSCN was carried out as explained in Section 3.6.

The long-term high stability of the core-shell MNPs synthesized via Method II is quite noteworthy and can be observed in Fig. 19B. For comparison, another batch of core-shell MNPs which were synthesized by different reaction parameters and were not stable under acidic conditions is shown in the same image. When Fe³⁺ releases from the core of the NPs and forms a complex with thiocyanate, it gives rise to a dark red coloration of the solution, indicating the leaching of iron.

Fig. 19 also shows that after the encapsulation of Fe₃O₄ MNPs with SiO₂, the material turned brownish and became dark beige after the surface functionalization with the IDA-derivate ligand. A previous study showed that the SiO₂ encapsulation of Fe₃O₄ MNPs leads to a quantitative oxidation of Fe₃O₄ to γ -Fe₂O₃ without significant loss in magnetic properties (Pogorilyi et al., 2014)

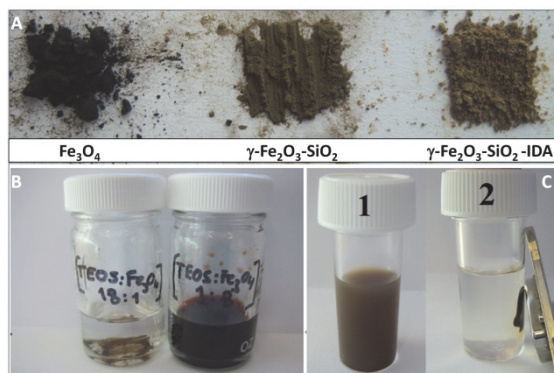


Figure 19. A: Difference in colours of the MNPs after different chemical treatment; B: Leaching test of the synthesized γ -Fe₂O₃-SiO₂ NPs; C: Magnetic removal of γ -Fe₂O₃-SiO₂ NPs

4.5 RE³⁺ Adsorption kinetic curves

4.5.1 Ligand grafted SiO₂ NPs (Paper I)

The kinetic curves obtained by complexometric titration as explained in section 3.8 show a quick achievement of the lanthanide adsorption equilibria, reaching over a 75% of the total capacity in less than 1h (Fig. 20). A quicker and higher uptake capacity can be observed for SiO₂ NPs functionalized with ligand 3, showing an uptake of 0.19 mmol Dy³⁺/g and 0.12 mmol Nd³⁺/g in 2 hours. The uptake capacity is, in this case, very reasonable for a static sorption process, resulting in an efficient material comparable to ion-exchange resins (El-Sofany,2008, Texier et al.,1999). For industrial purposes, usually an uptake capacity of 30mg/g or higher is required. In this work, this limit has been reached and surpassed, at least for Dy³⁺ with a capacity of 0.19 mmol Dy³⁺/g, equivalent to 30.9 mg Dy³⁺/g.

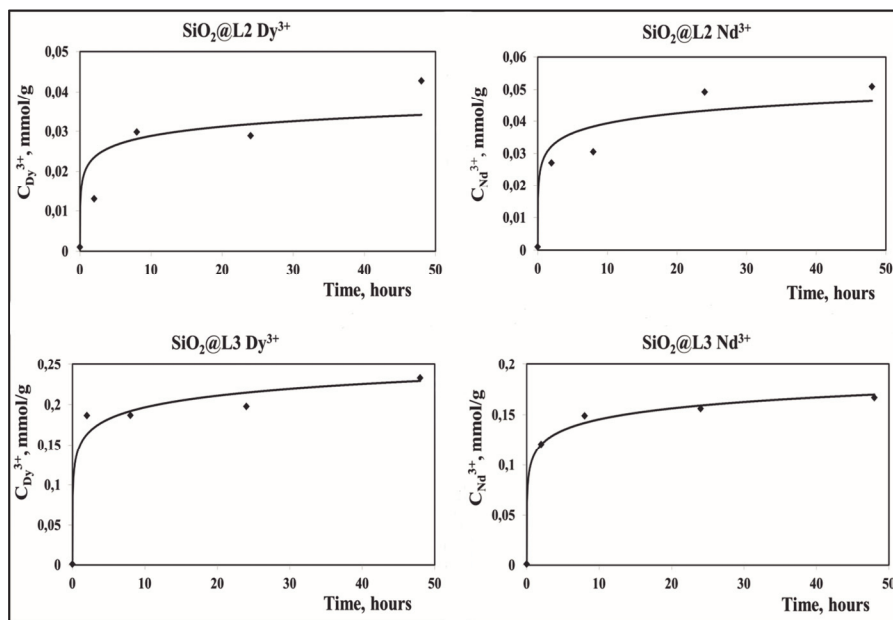


Figure 20. Kinetic adsorption curves for Dy³⁺ and Nd³⁺ on ligand grafted SiO₂ NPs.

4.5.2 Ligand grafted $\gamma\text{-Fe}_2\text{O}_3\text{-SiO}_2$ MNPs

The kinetic curves for these nanoadsorbents show as well a quick achievement of the adsorption equilibria (Fig. 21), reaching in the three investigated cases (Dy^{3+} , Nd^{3+} and La^{3+}) more than 65% of the maximum uptake in 2 hours.

Uptake capacity is, for the three RE cations very reasonable and effective. The best uptake capacity is displayed towards Dy^{3+} cations, with a maximum uptake of 0.25 mmol Dy^{3+}/g (equivalent to 40 mg Dy^{3+}/g), whereas the maximum uptake for Nd^{3+} is 0.23 mmol Nd^{3+}/g (equivalent to 33.6 mg Nd^{3+}/g) and 0.20 mmol La^{3+}/g (equivalent to 27.8 mg La^{3+}/g) in the case of La^{3+} .

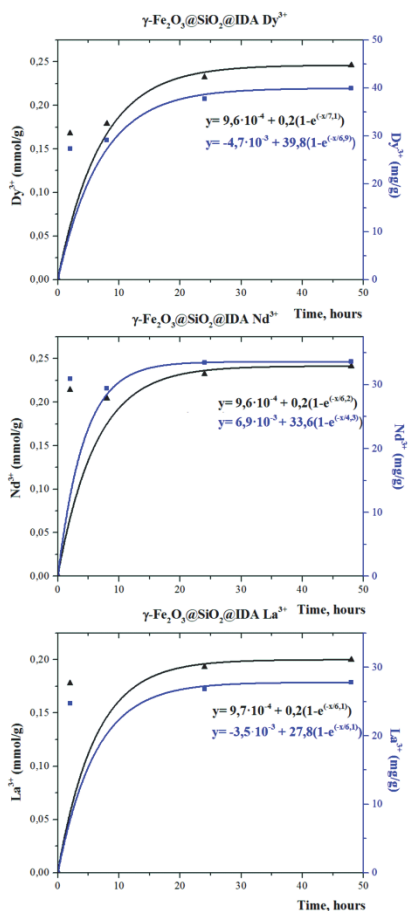


Figure 21. Kinetic curves of Dy^{3+} , Nd^{3+} and La^{3+} static sorption process on $\gamma\text{-Fe}_2\text{O}_3\text{-SiO}_2\text{-L3}$ NPs (mmol RE^{3+}/g in black and mg RE^{3+}/g in blue)

4.6 Desorption and selectivity studies (Paper I & II)

Desorption efficiency under acidic conditions (HNO₃ 1M) of the nanoadsorbent materials bearing RE³⁺ was tested. Table 3 shows the achieved percentage desorbed into solution, showing a high efficiency in the process, with more than 80% desorbed in all cases and in most of them well over 90%.

Table 3. Desorption efficiency for different materials bearing RE³⁺ cations

Sample	Percentage desorbed (%)
SiO ₂ -L3-Dy ³⁺	83
SiO ₂ -L3-Nd ³⁺	93.1
γ-Fe ₂ O ₃ -SiO ₂ -L3-Dy ³⁺	91.3
γ-Fe ₂ O ₃ -SiO ₂ -L3-Nd ³⁺	98.4
γ-Fe ₂ O ₃ -SiO ₂ -L3-La ³⁺	93.9

In the case of γ-Fe₂O₃-SiO₂-L3 MNPs, the amount of RE ions adsorbed was comparable but distinctly different, with a higher capacity towards heavier REE with smaller ionic radius. This indicated the possibility of selective adsorption in complex solutions. In order to investigate this, experiments of adsorption with binary mixtures (La-Dy and Dy-Nd) were performed. The particles saturated with RE cations were afterwards subjected to desorption processes at pH= 3.0 and pH= 1.0. The different metal ratios obtained under these two desorption conditions are summarized in Table 4.

Table 4. Capacity and selectivity in adsorption and desorption of RE cations

	Dy:Nd ratio	Dy:La ratio
Particles obtained after adsorption at neutral pH	3.9 : 1	4.2 : 1
Particles obtained after desorption at pH=3	5.9 : 1	81 : 1
Particles obtained after desorption at pH=1	1.3 : 1	1.8 : 1
Total uptake capacity (mmol RE ³⁺ /g)	0.242	0.275

These results provide proof of a quite appreciable selectivity towards Dy^{3+} , especially in the case of desorption at $\text{pH}=3.0$ from La-Dy binary mixture. The enrichment factor in adsorption for both Dy-Nd and Dy-La binary mixtures are quite close to that observed for La-Dy binary mixture reported in parallel with us by Binnemans and co-workers (Dupont et al., 2014).

4.6.1 Molecular insights into the observed selectivity (Paper II)

The molecular models, synthesized as explained in section 3.7 were studied by single crystal X-Ray diffraction. The composition of the surface complexes is $M : L = 1 : 1$. The analysis showed a flat layer coordination but with a remarked different coordination number depending on the REE studied (Fig. 22)

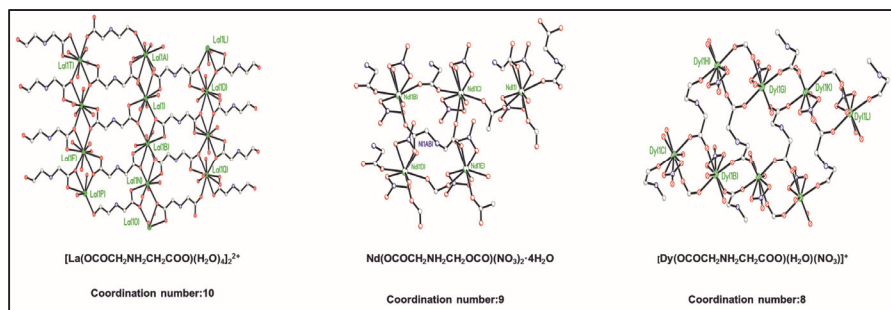


Figure 22. Structures of 2D coordination polymers as models for binding the REE in the surface layers with covalently grafted IDA molecules

The distances between the N-atoms attached to the siloxane centers vary depending on the REE, being 4.9\AA for La, 5.7\AA for Nd and 6.4\AA for Dy. In the view that, as reported in a previous study (Seisenbaeva et al., 2015), the distance between the Si-centers is at least 8.68\AA , the reasons for the observed selectivity towards Dy^{3+} in Dy-La case are apparent.

4.7 Testing on real solutions. Industrial Leachate from Fen Minerals.

The final aim of these magnetic silica based nanoadsorbents is to be able to apply them in a real industrial process of extraction and separation of REE. The work showed so far dealt with prepared model solutions, but the study of its applicability to real situations is one of the main targets of the project. Therefore, there is a collaborative network between research institutions and mining companies within the project, and some testing of the magnetic silica based nanoadsorbents on industrial leachate solutions has already started and is ongoing.

A leachate solution from the existing ore in Rødberg (Norway) was provided by Fen minerals. The leachate contained approximately a 70% of Ca and a 9% of Fe. The REE content was around 2%, assuming that Lanthanum and Cerium constitute 70% of the total REE amount.

The high content in calcium and iron constitutes a great challenge for selective and effective uptake of REE, which is why a chemical pre-treatment of the solution was carried out. This pre-treatment is summarized in Fig. 23 and includes a first step of precipitation of Calcium with ammonium sulfate and a further neutralization of the solution.

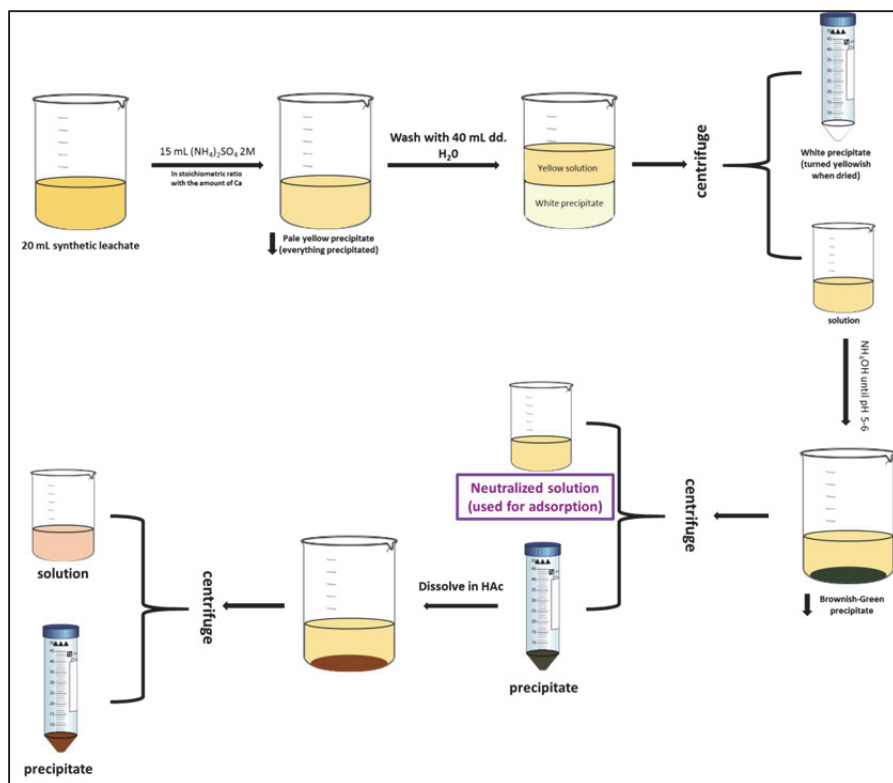


Figure 23. Scheme of the chemical pretreatment performed on the industrial leachate

Preliminary results showed that the pretreatment was well effective, obtaining a solution enriched in REE and eliminating most of the elements that may hinder the adsorption by magnetic silica nanoparticles. Uptake efficiency was also tested and showed to be preliminary reasonable. More detailed results can unfortunately not be provided yet due to confidentiality issues and the necessity of further work in this area.

5 Conclusions

In agreement with the main objectives of this thesis, novel hybrid magnetic silica based nanoadsorbents have been synthesized and surface decorated with three different organosilane derivatives, resulting in a material highly efficient for adsorption of REE in solution.

It has been demonstrated that hybrid SiO₂ NPs could be produced in reproducible way via surface grafting approach. These hybrid SiO₂ NPs were used as models for adsorption of REE for the later developed magnetic silica based nanoadsorbents. The obtained kinetic curves showed a quick and efficient uptake, especially for SiO₂-L3 NPs (where L3 was one of the IDA derivative ligand) towards Dy³⁺, in which case the adsorption efficiency was comparable to that obtained by ion exchange resins. Furthermore, luminescence studies of the hybrid SiO₂ NPs bearing RE³⁺ cations revealed the possibility of using them as a luminescent probe to detect Dy³⁺ and Nd³⁺ in solution.

The second part of this work demonstrated the advantages of using magnetic silica based nanoadsorbents, which awards a much easier removal. The organic reactant that proved to be the most suitable and efficient for REE adsorption in the first part of the work (Ligand 3) was used in this part to graft the surface of core-shell magnetic highly stable γ -Fe₂O₃-SiO₂ NPs. Adsorption efficiency towards RE³⁺ cations in solution was proved, revealing a very reasonable capacity. In this case, desorption efficiency under acidic (HNO₃ 1M) conditions was also tested, achieving more than 95% of desorption in most of the tested cases. Selectivity studies with binary RE mixtures were performed and showed that the magnetic silica nanoadsorbent exhibits a noteworthy selectivity towards Dy³⁺, especially in the case of Dy-La mixtures when they are desorbed at slightly mild conditions (pH=3), with a ratio Dy:La of 81:1. This enhanced selectivity was explained from a molecular point of view by the aid of single crystal X-ray crystallography. The binding at neutral

or weakly acidic conditions occurs apparently not via chelation but via concerted action of the negatively charged carboxylate atoms of the anions, which opens possibilities for a selective binding and release. It is also worth to point out that the obtained magnetic silica based nanoparticles were stable for more than a year under acidic conditions, which is very important for industrial purposes.

Lastly, a quick overview of the ongoing work with real industrial solutions was presented. Extraction and separation of REE in ore leachates becomes challenging since there are many hindering elements together with the REE. That is the reason why a chemical pre-treatment of the solution was carried out, in order to obtain an enriched solution in REE with which it would be easier to perform adsorption by the produced new hybrid nanoadsorbents. Preliminary results showed very promising perspectives for the further work that will be carried out in this PhD project.

6 Future prospects

As it has been proved with this work, magnetic silica based nanoadsorbents are very promising for efficient and selective extraction and separation of REE. These materials open a wide spectrum of applications and possibilities. The future work which will be carried out during the rest of this PhD project will be most likely directed to:

- Broadening the organic reactants library, hopefully achieving more efficient and selective hybrid nanoadsorbents.
- Optimizing desorption procedures, perhaps trying milder conditions for a whole environmentally friendlier process.
- Further and deep work with real industrial leachates, in order to achieve a viable selective and efficient extraction from them.

References

- ABBAS, M., RAO, B. P., ISLAM, M. N., NAGA, S. M., TAKAHASHI, M. & KIM, C. 2014. Highly stable- silica encapsulating magnetite nanoparticles (Fe₃O₄/SiO₂) synthesized using single surfactantless- polyol process. *Ceramics International*, 40, 1379-1385.
- ABSALAN, G., ASADI, M., KAMRAN, S., SHEIKHIAN, L. & GOLTZ, D. M. 2011. Removal of reactive red-120 and 4-(2-pyridylazo) resorcinol from aqueous samples by Fe₃O₄ magnetic nanoparticles using ionic liquid as modifier. *J Hazard Mater*, 192, 476-84.
- AI, H., FLASK, C., WEINBERG, B., SHUAI, X., PAGEL, M. D., FARRELL, D., DUERK, J. & GAO, J. 2005. Magnetite-loaded polymeric micelles as ultrasensitive magnetic-resonance probes. *Advanced Materials*, 17, 1949-1952.
- AL-SAYARI, S., CARLEY, A. F., TAYLOR, S. H. & HUTCHINGS, G. J. 2007. Au/ZnO and Au/Fe₂O₃ catalysts for CO oxidation at ambient temperature: Comments on the effect of synthesis conditions on the preparation of high activity catalysts prepared by coprecipitation. *Topics in Catalysis*, 44, 123-128.
- ALBORNOS, C. & JACOBO, S. E. 2006. Preparation of a biocompatible magnetic film from an aqueous ferrofluid. *Journal of Magnetism and Magnetic Materials*, 305, 12-15.
- AZHAR UDDIN, M., TSUDA, H., WU, S. & SASAOKA, E. 2008. Catalytic decomposition of biomass tars with iron oxide catalysts. *Fuel*, 87, 451-459.
- BADRUDDOZA, A. Z. M., SHAWON, Z. B. Z., TAY, W. J. D., HIDAJAT, K. & UDDIN, M. S. 2013. Fe₃O₄/cyclodextrin polymer nanocomposites for selective heavy metals removal from industrial wastewater. *Carbohydrate Polymers*, 91, 322-332.
- BASAK, S., CHEN, D.-R. & BISWAS, P. 2007. Electrospray of ionic precursor solutions to synthesize iron oxide nanoparticles: Modified scaling law. *Chemical Engineering Science*, 62, 1263-1268.
- BAUTISTA, F. M., CAMPELO, J. M., LUNA, D., MARINAS, J. M., QUIRÓS, R. A. & ROMERO, A. A. 2007. Screening of amorphous metal-phosphate

- catalysts for the oxidative dehydrogenation of ethylbenzene to styrene. *Applied Catalysis B: Environmental*, 70, 611-620.
- BRUNAUER, S., EMMETT, P. H. & TELLER, E. 1938. Adsorption of Gases in Multimolecular Layers. *Journal of the American Chemical Society*, 60, 309-319.
- BÜNZLI, J.-C. G. & PIGUET, C. 2002. Lanthanide-Containing Molecular and Supramolecular Polymetallic Functional Assemblies. *Chemical Reviews*, 102, 1897-1928.
- CHEN, Y., QIAN, H., WU, F. & ZHOU, J. 2011. Clearance and recovery of Cd(II) from aqueous solution by magnetic separation technology. *Chemosphere*, 83, 1214-9.
- CHIN, A. B. & YAACOB, I. I. 2007. Synthesis and characterization of magnetic iron oxide nanoparticles via w/o microemulsion and Massart's procedure. *Journal of Materials Processing Technology*, 191, 235-237.
- CLARAMUNT, R. M., ELGUERO, J., HERRANZ, F., PINILLA, E., SANTA MARIA, M. D. & TORRES, M. R. 2005. Molecular recognition of biotin, barbital and tolbutamide with new synthetic receptors.
- CORNELL, R. M. & SCHWERTMANN, U. 2003. *The iron oxides: structure, properties, reactions, occurrences and uses*, Weinheim, Germany, WILEY-VCH Verlag GMBH & Co. KGaA.
- DUDARKO, O. A., GONCHARIK, V. P., SEMENII, V. Y. & ZUB, Y. L. 2008. Sorption of Hg²⁺, Nd³⁺, Dy³⁺, and UO₂²⁺ ions at polysiloxane xerogels functionalized with phosphonic acid derivatives. *Protection of Metals*, 44, 193-197.
- DUPONT, D., BRULLOT, W., BLOEMEN, M., VERBIEST, T. & BINNEMANS, K. 2014. Selective Uptake of Rare Earths from Aqueous Solutions by EDTA-Functionalized Magnetic and Nonmagnetic Nanoparticles. *ACS Applied Materials & Interfaces*, 6, 4980-4988.
- EFFATI, E. & POURABBAS, B. 2012. One-pot synthesis of sub-50 nm vinyl- and acrylate-modified silica nanoparticles. *Powder Technology*, 219, 276-283.
- EL-SOFANY, E. A. 2008. Removal of lanthanum and gadolinium from nitrate medium using Aliquat-336 impregnated onto Amberlite XAD-4. *J Hazard Mater*, 153, 948-54.
- EURARE. 2013. *Development of a sustainable exploitation scheme for Europe's Rare Earth ore deposits* [Online]. Available: <http://www.eurare.eu/>.
- EUROPEAN COMMISSION, E. 2010. Critical Raw Materials for the EU. Report of the Ad-hoc Working group on Defining Critical Raw Materials. . *European Commission, Enterprise and Industry*
- FANG, Z., QIU, X., CHEN, J. & QIU, X. 2011a. Degradation of the polybrominated diphenyl ethers by nanoscale zero-valent metallic particles prepared from steel pickling waste liquor. *Desalination*, 267, 34-41.
- FANG, Z., QIU, X., HUANG, R., QIU, X. & LI, M. 2011b. Removal of chromium in electroplating wastewater by nanoscale zero-valent metal with synergistic effect of reduction and immobilization. *Desalination*, 280, 224-231.

- FARAJI, M., YAMINI, Y. & REZAEI, M. 2010. Magnetic Nanoparticles: Synthesis, Stabilization, Functionalization, Characterization, and Applications. *Journal of the Iranian Chemical Society*, 7, 1-37.
- FRANVILLE, A. C., ZAMBON, D., MAHIOU, R., CHOU, S., TROIN, Y. & COUSSEINS, J. C. 1998. Synthesis and optical features of an europium organic-inorganic silicate hybrid. *Journal of Alloys and Compounds*, 275-277, 831-834.
- GONZAGA, F., YU, G. & BROOK, M. A. 2009. Versatile, efficient derivatization of polysiloxanes via click technology. *Chemical Communications*, 1730-1732.
- GONZALES, M. & KRISHNAN, K. M. 2005. Synthesis of magnetoliposomes with monodisperse iron oxide nanocrystal cores for hyperthermia. *Journal of Magnetism and Magnetic Materials*, 293, 265-270.
- GUPTA, A. K. & GUPTA, M. 2005. Synthesis and surface engineering of iron oxide nanoparticles for biomedical applications. *Biomaterials*, 26, 3995-4021.
- HEE KIM, E., SOOK LEE, H., KOOK KWAK, B. & KIM, B.-K. 2005. Synthesis of ferrofluid with magnetic nanoparticles by sonochemical method for MRI contrast agent. *Journal of Magnetism and Magnetic Materials*, 289, 328-330.
- HURST, C. 2010. China's Rare Earth Element Industry: What Can the West Learn? : Institute for the Analysis of Global Security.
- IM, S. H., HERRICKS, T., LEE, Y. T. & XIA, Y. 2005. Synthesis and characterization of monodisperse silica colloids loaded with superparamagnetic iron oxide nanoparticles. *Chemical Physics Letters*, 401, 19-23.
- IRAM, M., GUO, C., GUAN, Y., ISHFAQ, A. & LIU, H. 2010. Adsorption and magnetic removal of neutral red dye from aqueous solution using Fe₃O₄ hollow nanospheres. *Journal of Hazardous Materials*, 181, 1039-1050.
- IUPAC 2005. *Nomenclature of Inorganic Chemistry. IUPAC Recommendations 2005.*, Cambridge, UK.
- JIANG, J. Z., ZOU, J., ZHU, L. H., HUANG, L., JIANG, H. P. & ZHANG, Y. X. 2011. Degradation of Methylene Blue with H₂O₂ Activated by Peroxidase-Like Fe₃O₄ Magnetic Nanoparticles. *Journal of Nanoscience and Nanotechnology*, 11, 4793-4799.
- JIN, T., INOUE, S., MACHIDA, K. & ADACHI, G. 1997. Photovoltaic cell characteristics of hybrid silicon devices with lanthanide complex phosphor-coating film. *Journal of the Electrochemical Society*, 144, 4054-4058.
- JURGONS, R., SELIGER, C., HILPERT, A., TRAHMS, L., ODENBACH, S. & ALEXIOU, C. 2006. Drug loaded magnetic nanoparticles for cancer therapy. *Journal of Physics Condensed Matter*, 18, S2893-S2902.
- KIMATA, M., NAKAGAWA, D. & HASEGAWA, M. 2003. Preparation of monodisperse magnetic particles by hydrolysis of iron alkoxide. *Powder Technology*, 132, 112-118.

- LEE, H., SHAO, H., HUANG, Y. & KWAK, B. 2005. Synthesis of MRI contrast agent by coating superparamagnetic iron oxide with chitosan. *IEEE Transactions on Magnetics*, 41, 4102-4104.
- LI, C., SHEN, Y., JIA, M., SHENG, S., ADEBAJO, M. O. & ZHU, H. 2008. Catalytic combustion of formaldehyde on gold/iron-oxide catalysts. *Catalysis Communications*, 9, 355-361.
- LIU, T.-H. 2004. Preparation and characterization of nano-structured silica from rice husk. *Materials Science and Engineering: A*, 364, 313-323.
- LU, A.-H., SALABAS, E. L. & SCHÜTH, F. 2007a. Magnetic Nanoparticles: Synthesis, Protection, Functionalization, and Application. *Angewandte Chemie International Edition*, 46, 1222-1244.
- LU, C.-W., HUNG, Y., HSIAO, J.-K., YAO, M., CHUNG, T.-H., LIN, Y.-S., WU, S.-H., HSU, S.-C., LIU, H.-M., MOU, C.-Y., YANG, C.-S., HUANG, D.-M. & CHEN, Y.-C. 2007b. Bifunctional Magnetic Silica Nanoparticles for Highly Efficient Human Stem Cell Labeling. *Nano Letters*, 7, 149-154.
- LÜBBE, A. S., BERGEMANN, C., BROCK, J. & MCCLURE, D. G. 1999. Physiological aspects in magnetic drug-targeting. *Journal of Magnetism and Magnetic Materials*, 194, 149-155.
- MAJEWSKI, P. 2008. *Maghemite* [Online]. Encyclopaedia Britannica Online: Encyclopaedia Britannica Online. Available: <http://search.eb.com/eb/article-9049986>.
- MAJEWSKI, P. & THIERRY, B. 2007. Functionalized Magnetite Nanoparticles—Synthesis, Properties, and Bio-Applications. *Critical Reviews in Solid State and Materials Sciences*, 32, 203-215.
- MARTÍNEZ-MERA, I., ESPINOSA-PESQUEIRA, M. E., PÉREZ-HERNÁNDEZ, R. & ARENAS-ALATORRE, J. 2007. Synthesis of magnetite (Fe₃O₄) nanoparticles without surfactants at room temperature. *Materials Letters*, 61, 4447-4451.
- MASSARI, S. & RUBERTI, M. 2013. Rare earth elements as critical raw materials: Focus on international markets and future strategies. *Resources Policy*, 38, 36-43.
- MEL'NIK, I. V., ZUB, Y. L., ALONSO, B., ABRAMOV, N. V. & GORBIK, P. P. 2012. Creation of a functional polysiloxane layer on the surface of magnetic nanoparticles using the sol-gel method. *Glass Physics and Chemistry*, 38, 96-104.
- MELNYK, I., GONCHARYK, V., STOLYARCHUK, N., KOZHARA, L., LUNOCHKINA, A., ALONSO, B. & ZUB, Y. 2012. Dy(III) sorption from water solutions by mesoporous silicas functionalized with phosphonic acid groups. *Journal of Porous Materials*, 19, 579-585.
- MELNYK, I. V. & ZUB, Y. L. 2012. Preparation and characterization of magnetic nanoparticles with bifunctional surface layer ≡Si(CH₂)₃NH₂/≡SiCH₃ (or ≡SiC₃H₇-n). *Microporous and Mesoporous Materials*, 154, 196-199.
- NASSAR, N. N. 2010. Rapid removal and recovery of Pb(II) from wastewater by magnetic nanoadsorbents. *Journal of Hazardous Materials*, 184, 538-546.

- PARKER, D. & BRETONNIERE, Y. 2005. Luminescent Lanthanide Complexes as Sensors and Imaging Probes. In: BOGDANOV, A. A., JR. & LICHA, K. (eds.) *Molecular Imaging*. Springer Berlin Heidelberg.
- PENG, C., ZHANG, H., YU, J., MENG, Q., FU, L., LI, H., SUN, L. & GUO, X. 2005. Synthesis, Characterization, and Luminescence Properties of the Ternary Europium Complex Covalently Bonded to Mesoporous SBA-15. *The Journal of Physical Chemistry B*, 109, 15278-15287.
- PINES, A., GIBBY, M. G. & WAUGH, J. S. 1973. Proton-enhanced NMR of dilute spins in solids. *The Journal of Chemical Physics*, 59, 569-590.
- POGORILYI, R. P., MELNYK, I. V., ZUB, Y. L., CARLSON, S., DANIEL, G., SVEDLINDH, P., SEISENBAEVA, G. A. & KESSLER, V. G. 2014. New product from old reaction: uniform magnetite nanoparticles from iron-mediated synthesis of alkali iodides and their protection from leaching in acidic media. *Rsc Advances*, 4, 22606-22612.
- PURI, J. K., SINGH, R., CHAHAL, V. K., SHARMA, R. P., WAGLER, J. & KROKE, E. 2011. New silatranes possessing urea functionality: Synthesis, characterization and their structural aspects. *Journal of Organometallic Chemistry*, 696, 1341-1348.
- QIANG, Y., ANTONY, J., SHARMA, A., NUTTING, J., SIKES, D. & MEYER, D. 2006. Iron/iron oxide core-shell nanoclusters for biomedical applications. *Journal of Nanoparticle Research*, 8, 489-496.
- QIU, J., YANG, R., LI, M. & JIANG, N. 2005. Preparation and characterization of porous ultrafine Fe₂O₃ particles. *Materials Research Bulletin*, 40, 1968-1975.
- RAKSHAE, R. & PANAHANDEH, M. 2011. Stabilization of a magnetic nano-adsorbent by extracted pectin to remove methylene blue from aqueous solution: A comparative studying between two kinds of cross-liked pectin. *Journal of Hazardous Materials*, 189, 158-166.
- RASHEED, Q. J., PANDIAN, K. & MUTHUKUMAR, K. 2011. Treatment of petroleum refinery wastewater by ultrasound-dispersed nanoscale zero-valent iron particles. *Ultrason Sonochem*, 18, 1138-42.
- REISS, G. & HUTTEN, A. 2005. Magnetic nanoparticles - Applications beyond data storage. *Nature Materials*, 4, 725-726.
- SADEGHIANI, N., BARBOSA, L. S., GLIEDES, M. H. A., CHAVES, S. B., SANTOS, J. G., SILVA, O., PELEGRINI, F., AZEVEDO, R. B., MORALS, P. C. & LACAVALA, Z. G. M. 2005. Magnetic resonance of polyaspartic acid-coated magnetite nanoparticles administered in mice. *IEEE Transactions on Magnetics*, 41, 4108-4110.
- SALAZAR-ALVAREZ, G., MUHAMMED, M. & ZAGORODNI, A. A. 2006. Novel flow injection synthesis of iron oxide nanoparticles with narrow size distribution. *Chemical Engineering Science*, 61, 4625-4633.
- SANTRA, S., TAPEC, R., THEODOROPOULOU, N., DOBSON, J., HEBARD, A. & TAN, W. 2001. Synthesis and Characterization of Silica-Coated Iron Oxide Nanoparticles in Microemulsion: The Effect of Nonionic Surfactants. *Langmuir*, 17, 2900-2906.
- SEISENBAEVA, G. A., MELNYK, I. V., HEDIN, N., CHEN, Y., ERIKSSON, P., TRZOP, E., ZUB, Y. L. & KESSLER, V. G. 2015. Molecular insight into

- the mode-of-action of phosphonate monolayers as active functions of hybrid metal oxide adsorbents. Case study in sequestration of rare earth elements. *RSC Advances*, 5, 24575-24585.
- SHAHRIARI, T., BIDHENDI, G. N., MEHRDADI, N. & TORABIAN, A. 2014. Effective parameters for the adsorption of chromium(III) onto iron oxide magnetic nanoparticle. *International Journal of Environmental Science and Technology*, 11, 349-356.
- SHARMA, R. K. & SHARMA, S. 2014. Silica nanosphere-supported palladium(II) furfural complex as a highly efficient and recyclable catalyst for oxidative amination of aldehydes. *Dalton Trans*, 43, 1292-304.
- SHEN, H., PAN, S., ZHANG, Y., HUANG, X. & GONG, H. 2012. A new insight on the adsorption mechanism of amino-functionalized nano-Fe₃O₄ magnetic polymers in Cu(II), Cr(VI) co-existing water system. *Chemical Engineering Journal*, 183, 180-191.
- SHEN, Y. F., TANG, J., NIE, Z. H., WANG, Y. D., REN, Y. & ZUO, L. 2009. Preparation and application of magnetic Fe₃O₄ nanoparticles for wastewater purification. *Separation and Purification Technology*, 68, 312-319.
- SHI, F., TSE, M. K., POHL, M. M., BRÜCKNER, A., ZHANG, S. & BELLER, M. 2007. Tuning catalytic activity between homogeneous and heterogeneous catalysis: Improved activity and selectivity of free nano-Fe₂O₃ in selective oxidations. *Angewandte Chemie - International Edition*, 46, 8866-8868.
- SHIBASAKI, M. & YOSHIKAWA, N. 2002. Lanthanide complexes in multifunctional asymmetric catalysis. *Chemical Reviews*, 102, 2187-2209.
- SILVERSTEIN RM, B. G., MORRILL TC 1981. Infrared spectrometry. In: Spectrometric identification of organic compounds
- SOENEN, S. J., DE CUYPER, M., DE SMEDT, S. C. & BRAECKMANS, K. 2012. Chapter ten - Investigating the Toxic Effects of Iron Oxide Nanoparticles. In: NEJAT, D. (ed.) *Methods in Enzymology*. Academic Press.
- STJERND AHL, M., ANDERSSON, M., HALL, H. E., PAJEROWSKI, D. M., MEISEL, M. W. & DURAN, R. S. 2008. Superparamagnetic Fe₃O₄/SiO₂ Nanocomposites: Enabling the Tuning of Both the Iron Oxide Load and the Size of the Nanoparticles. *Langmuir*, 24, 3532-3536.
- STÖBER, W., FINK, A. & BOHN, E. 1968. Controlled growth of monodisperse silica spheres in the micron size range. *Journal of Colloid and Interface Science*, 26, 62-69.
- TARN, D., XUE, M. & ZINK, J. I. 2013. pH-responsive dual cargo delivery from mesoporous silica nanoparticles with a metal-latched nanogate. *Inorg Chem*, 52, 2044-9.
- TARTAJ, P., DEL PUERTO MORALES, M., VEINTEMILLAS-VERDAGUER, S., GONZÁLEZ-CARREÑO, T. & SERNA, C. J. 2003. The preparation of magnetic nanoparticles for applications in biomedicine. *Journal of Physics D: Applied Physics*, 36, R182-R197.

- TEJA, A. S. & KOH, P.-Y. 2009. Synthesis, properties, and applications of magnetic iron oxide nanoparticles. *Progress in Crystal Growth and Characterization of Materials*, 55, 22-45.
- TEXIER, A.-C., ANDRÈS, Y. & LE CLOIREC, P. 1999. Selective Biosorption of Lanthanide (La, Eu, Yb) Ions by *Pseudomonas aeruginosa*. *Environmental Science & Technology*, 33, 489-495.
- THANH, N. T. K. 2012. *Magnetic Nanoparticles: From Fabrication to Clinical Applications*, London, CRC Press.
- TU, Y. J., YOU, C. F. & CHANG, C. K. 2012. Kinetics and thermodynamics of adsorption for Cd on green manufactured nano-particles. *J Hazard Mater*, 235-236, 116-22.
- WAN, J., CHEN, X., WANG, Z., YANG, X. & QIAN, Y. 2005. A soft-template-assisted hydrothermal approach to single-crystal Fe₃O₄ nanorods. *Journal of Crystal Growth*, 276, 571-576.
- WANG, C. T. & WILLEY, R. J. 1998. Oxidation of methanol over iron oxide based aerogels in supercritical CO₂. *Journal of Non-Crystalline Solids*, 225, 173-177.
- WANG, Y. & DAVIS, B. H. 1999. Fischer-Tropsch synthesis. Conversion of alcohols over iron oxide and iron carbide catalysts. *Applied Catalysis A: General*, 180, 277-285.
- WILKINSON, K., EKSTRAND-HAMMARSTROM, B., AHLINDER, L., GULDEVALL, K., PAZIK, R., KEPINSKI, L., KVASHNINA, K. O., BUTORIN, S. M., BRISMAR, H., ONFELT, B., OSTERLUND, L., SEISENBAEVA, G. A. & KESSLER, V. G. 2012. Visualization of custom-tailored iron oxide nanoparticles chemistry, uptake, and toxicity. *Nanoscale*, 4, 7383-7393.
- XU, P., ZENG, G. M., HUANG, D. L., LAI, C., ZHAO, M. H., WEI, Z., LI, N. J., HUANG, C. & XIE, G. X. 2012. Adsorption of Pb(II) by iron oxide nanoparticles immobilized *Phanerochaete chrysosporium*: Equilibrium, kinetic, thermodynamic and mechanisms analysis. *Chemical Engineering Journal*, 203, 423-431.
- XU, Z. P., ZENG, Q. H., LU, G. Q. & YU, A. B. 2006. Inorganic nanoparticles as carriers for efficient cellular delivery. *Chemical Engineering Science*, 61, 1027-1040.
- YURCHENKO, G. R., MATKOVSKII, A. K., MEL'NIK, I. V., DUDARKO, O. A., STOLYARCHUK, N. V., ZUB, Y. L. & ALONSO, B. 2012. Adsorption properties of silica-based sorbents containing phosphonic acid residues. *Colloid Journal*, 74, 386-390.
- ZHANG, H., ZHAO, Z., XU, X. & LI, L. 2011. Study on industrial wastewater treatment using superconducting magnetic separation. *Cryogenics*, 51, 225-228.
- ZHANG, P., ZHANG, L., WANG, C., XUE, S. F., LIN, S. Y. & TANG, J. K. 2014. Equatorially Coordinated Lanthanide Single Ion Magnets. *Journal of the American Chemical Society*, 136, 4484-4487.
- ZHANG, R., HUANG, J., ZHAO, J., SUN, Z. & WANG, Y. 2007. Sol-gel auto-combustion synthesis of zinc ferrite for moderate temperature desulfurization. *Energy and Fuels*, 21, 2682-2687.

ZHENG, Y. H., CHENG, Y., BAO, F. & WANG, Y. S. 2006. Synthesis and magnetic properties of Fe₃O₄ nanoparticles. *Materials Research Bulletin*, 41, 525-529.

Acknowledgements

There are so many people towards whom I feel extremely grateful for making this journey enjoyable and less tough, that I apologize in advance if I forget any of them. I promise I am going to do my best not to, and to make the best use of the following lines to express my gratitude to everyone that has been important during these two years.

Firstly, I would like to express my deepest gratitude to my main supervisor **Gulaim A. Seisenbaeva**, who I truly admire, not only as the great scientist she is, but also as a loving and caring woman. Gulaim, thank you for teaching me everything I know so far in research, I am looking forward to keep learning from you every day, and thanks for always caring about me, not only in my scientific development but also in my personal life.

Thanks to my co-supervisor, **Vadim G. Kessler**, who also has my full admiration and respect both professionally and personally. Vadim, thank you for always having a word of support and belief in me when I most needed it. I feel very thankful to be under the guidance of both of you, and hope to make the most out of the remaining time of my PhD. Спасибо большое!

Thanks to my previous supervisors and mentors in University of Navarre, University of Malaga and Florida International University for arousing my interest in research and always believe in me. **Carolina Santamaría, José María Fernández, Tomás Cordero and José R. Almirall**, thanks for encouraging me to pursue PhD studies. This would have never happened without your help.

To the person who made my start as a PhD student much easier and smoother, **Seda Demirel Topel**, thank you very much! I learnt a lot from you and spent very memorable times with you in the lab. Çok teşekkürler!

Leaving my home country, more or less “forever”, for a 23 year old girl as I was in 2013, was not exactly an easy decision, and while it has certainly been no bed of roses, it’s been definitely much easier and pleasant thanks to all the amazing people that I work with. Nowadays, I can firmly claim that I am very happy to have made this move in my life, and you, my wonderful colleagues, are a big part of this.

Starting from my room mates: **Martin Palmqvist**, who by now is almost like my brother (although my real sister might still hold a grudge against you :P), you have been one of my greatest supports during my ups and downs, and for that I am extremely thankful to you, also for your patience to teach me swedish and your encouragement to try to make me speak it! Tack! ☺ Thanks as well for the nice ping-pong games as a stress reliever therapy. Now I can finally leave written proof of the historic day and time on which I won a ping-pong game against Martin Palmqvist, 16th of November 2015 at 18:26 (you can try to fade away your memories, but ink won’t fade you know!).

Tobias Bölscher, thank you very much for your patience and enjoyable company in the office. My best wishes for your PhD!

Hanna Eriksson, big thanks for very nice conversations in the coffee room, getting to know you a bit more was a pleasure and it always helps to know that you are not the only one sometimes struggling with too much stress. We will manage! ☺

Anke Herrman, you are just awesome! Thanks for always having a smile on your face and be willing to listen to me.

Yina Salamanca, gracias por estar ahí, por acogerme en tu casa y siempre ayudarme. Te deseo muchísima suerte en todo lo que hagas y un feliz futuro ☺.

Alexandra Olarte, gracias por contagiarme tu alegría y por tus deliciosos cócteles ☺. Espero tenerte por aquí mucho tiempo!

Sonja Jansson, thank you very much for always being kind and helpful with all my questions about administrative work. Thanks for your endless patience in speaking slowly and easy swedish to me to help me learning.

Karin Örneby, thank you for your energy and for always caring about me!

Frida Wende, Lena Lundqvist, Christina Nord, thank you girls for always having a smile and a nice word for me. I promise you that one day I will be able to sit with you in the coffee room and have a conversation in perfect Swedish! ☺

Elisabeth Müllner, thanks for being such a kind and easy to talk to person. I wish you, and **Ali Moazzami** all the happiness with the soon coming of your daughter and a successful professional future.

Ingmar Persson, thanks for sharing with us part of your brilliant knowledge and teaching us about the fascinating world of inorganic chemistry.

Thanks to **Peter Agback** for help with NMR, to **Gunnar Almkvist, Anna Borisova, Jule Brandenburg, Camila Demmou, Emad Ehtesham, Daniel Lundberg, Benjamin Schmuck, Corinne Sandström, Anders Sandström, Jerry Ståhlberg**, and everyone in the **Department of Chemistry and Biotechnology** for being the best company that one could ever work with ☺

Now the most difficult part starts...expressing my gratitude to all my family and friends. I would need pages and pages to thank everyone that has been important during this time, so please do not take offense if you don't find yourself in these lines. If you are part of my life, you can be fully sure that I feel lucky and thankful to have you.

Mamá, cualquier palabra que escribiese no sería suficiente para expresar todo lo que tengo que agradecerte. Gracias por tu amor incondicional, por haberme criado para ser la persona que hoy soy y por siempre querer lo mejor para mí, incluso si eso significa tenerme a 3000 km de distancia.

Lo mismo se aplica a ti, **Papá**, gracias por siempre estar orgulloso de mí, por haber luchado siempre para que nunca nos faltase nada y tuviésemos todo lo que vosotros no pudisteis tener. Sin vuestro esfuerzo, nunca habríamos llegado a donde, tanto la Cris como yo, hemos llegado.

Hermana, no sabría ni por dónde empezar...así que igual mejor no lo hago, ¿no? :P Es bromi, no quiero ponerme moñas que luego te me acostumbras, pero gracias por ser la mejor hermana del mundo, por no tener jamás un sentimiento malo hacia mí y por aguantarme, que no es poco. Gracias, hermanapamplonesatonta!

Gracias a toda mi familia, primos, tíos, y los tres principitos que espero que dentro de unos años puedan leer esto. Gracias a todos por ser la mejor familia que alguien podría tener!

To my dearest friend **Olga Galkina**, I would need a whole book to express how thankful I feel to have your priceless friendship. I never thought I would meet someone with such a kind and truly good heart as yours. My Олечка, you are the best friend one could ever ask for. I wish that life brings you all the good things that you deserve.

Philip Eriksson, thanks for your constant happiness and energy! I wish you the best for your future.

A **Miguel**, quien es una de las personas más importantes para mí, mi mayor confidente y consejero. Gracias por ser tú, no dejes de serlo nunca :P.

A mi amiga **Saioa**, porque aunque no nos veamos muy a menudo, cuando lo hacemos es como si no hubiera pasado el tiempo. Gracias, Zaio!

A todos mis amigos tanto en España como en Uppsala, por hacerme sentir que tengo una parte de mi corazón y de mi vida en ambos lugares.

Last but absolutely not least, to my dear **Jon**, who has been the one to suffer all my breakdowns and stress. I apologize for having been such a hard piece of work lately and I heartfelt thank you for being there, supporting me and always having a smile for me. I feel extremely lucky to have found such an incredible person as you are and to have you in my life. Tack för allt, guapo ☺.

*Eli,
Uppsala, December 2015*